Structures and Properties of a Series of High-Spin [Co^{II}_2] Complexes Supported by Ancillary Benzoate, *Ortho*-Hydroxybenzoate, and *Para*-Hydroxybenzoate Ligands

Sujan Sk, Samik Biswas, Nityananda Dutta, Arpan Das, Nithin Suryadevara, Gonela Vijaykumar, Pradip Bhunia, Mario Ruben, Supratim Mandal, and Manindranath Bera*

ABSTRACT: A new series of high-spin [Co^{II}_2] complexes [Co_2(cpdp)(μ-$O_2CC_6H_5$)] (**1**), [Co_2(cpdp)(μ-*o*-$O_2CC_6H_4$-(OH))]·H_2O (**2**), a nd [Co_2(cpdp)(μ-*p*-$O_2CC_6H_4$(OH))]·$5H_2O$ (**3**) of the carboxylate-affixed multidentate ligand, *N*,*N*′-bis[2-carboxybenzomethyl]-*N*,*N*′-bis[2-pyridylmethyl]-1,3-diaminopropan-2-ol (H_3cpdp), have been synthesized and structurally characterized [$C_6H_5CO_2^-$ = benzoate; *o*-C_6H_4(OH)CO_2^- = *ortho*-hydroxybenzoate; *p*-C_6H_4(OH)CO_2^- = *para*-hydroxybenzoate]. In methanol, complexes **1**, **2**, and **3** have been synthesized by carrying out the reaction of H_3cpdp with stoichiometric quantities of $Co(BF_4)_2$·$6H_2O$/$C_6H_5CO_2Na$, $Co(BF_4)_2$·$6H_2O$/*o*-C_6H_4(OH)CO_2Na, and $Co(BF_4)_2$·$6H_2O$/*p*-C_6H_4(OH)CO_2Na respectively, in the presence of NaOH at room temperature. Complexes **1**−**3** have been characterized by microanalysis, molar conductance, FTIR and UV−vis, mass spectrometry, PXRD, thermogravimetric analysis, single-crystal X-ray diffraction studies, and variable temperature magnetic susceptibility measurements. In **1**−**3**, the nonbonded Co···Co separations are 3.4311(8), 3.4551(8), and 3.4393(7) Å, respectively, and the Co(II) ions are doubly bridged by one alkoxide group of the multidentate ligand and one benzoate/*ortho*-hydroxybenzoate/*para*-hydroxybenzoate group. As disclosed by single-crystal X-ray analyses, all three complexes assume distorted trigonal bipyramidal geometry around each cobalt center under the N_2O_3 coordination environment provided by the $cpdp^{3-}$ ligand and the ancillary benzoate/*ortho*-hydroxybenzoate/*para*-hydroxybenzoate functionalities. The distorted trigonal bipyramidal geometry is further authenticated by SHAPE analysis of the Co(II) coordination sphere. Magnetic susceptibility data were recorded for **1**−**3** in the temperature range of 2−300 K, and their analysis has disclosed the occurrence of antiferromagnetic interactions, associated with the spin-orbit coupling effect. The nature and mechanism of magnetic interactions are discussed on the basis of magneto-structural parameters, and these are mainly correlated with the magnitude of Co−$O_{bridging\ alkoxide}$−Co angles. Moreover, with the aim of reducing toxicity and irritation of free cobalt(II) ion in the tissues, all three organo-chelated [Co^{II}_2] complexes were evaluated as antibacterial agents against *Staphylococcus aureus*, SA96, which is known to cause several life-threatening chronic infections and diseases. The antibacterial studies revealed that all three complexes are significantly active against this bacterial strain showing minimum inhibitory concentration values in the range of 300−600 μg/mL. However, a comparative assessment of their biological efficacies revealed that **2** and **3** exhibited higher antibacterial activity compared to that of **1**.

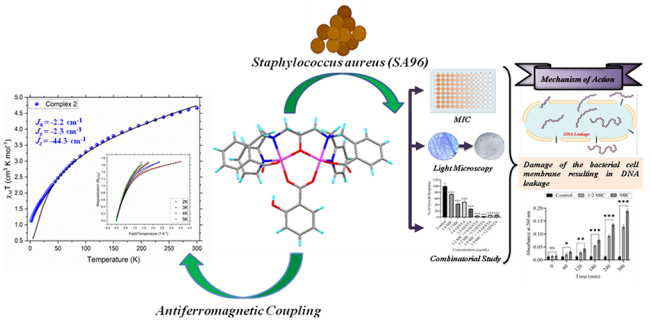

INTRODUCTION

Significant research endeavor has been directed toward synthesis and characterization of transition metal complexes since the 19th century with the discovery of Werner's theory. They have played a remarkable role in the development of numerous functional materials. They have also exhibited many interesting, challenging, and diverse coordination chemistry. Until now, considerable research and development of transition metal complexes is ongoing because of their tremendous applications and advances in the field of bioinorganic chemistry, medicinal chemistry, drug delivery, catalysis, gas sorption, sensing, and molecular magnetism.[1,2] These applications and advances have rekindled our interest in the synthesis and physicochemical characterization of different transition metal complexes. Among them, high-spin Co(II) complexes are very popular to the coordination/material chemists owing to their interesting magnetic properties.[3−7] They are good candidates that act as single-molecule

Chart 1. Depiction of Possible Coordination Modes Exhibited by H_3cpdp on Complexing with Metal Ions

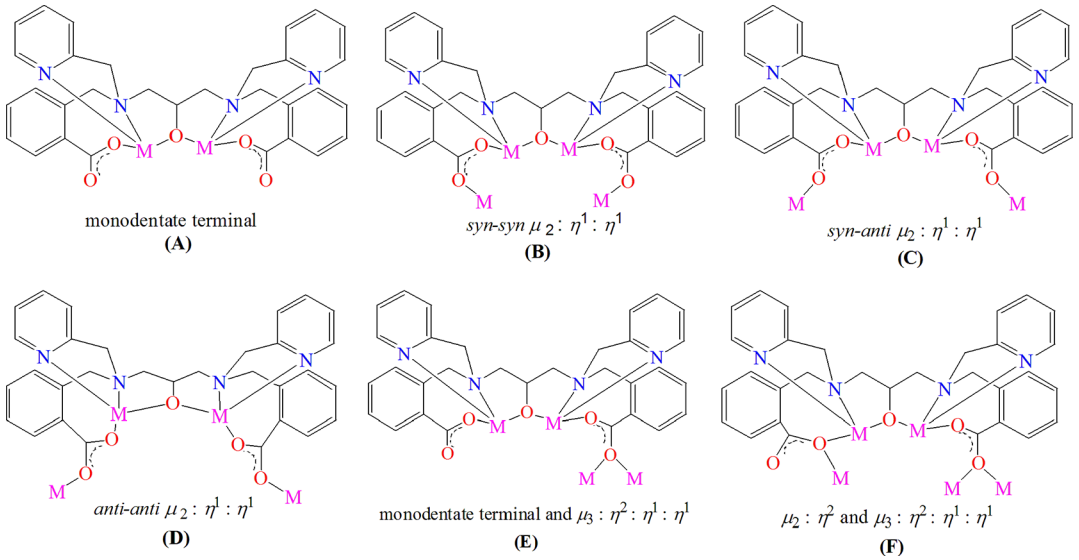

magnets[8,9] and single-chain magnets[10,11] because of their half-integer spins ($S = {}^3/_2$) and sizable magnetic anisotropy arising from spin-orbit coupling among the ligand field states.[12−16] Several studies on mono- and dinuclear Co(II) complexes have shown the impact of coordination number, geometrical arrangement, and identity of the ligand on zero-field splitting parameters and magnetic relaxation rates.[17−20] In this context, the dinuclear Co(II) complexes bearing alkoxide/phenoxide/hydroxide bridges have attracted much attention in recent times.[21−28] Particular interest has been focused on the relationship between their structures and magnetic properties in order to understand the detailed magneto-structural correlations.[29−33] It should be mentioned that the dimetallic complexes constitute an emerging and sophisticated subgroup of compounds within the family of multinuclear metal assemblies. Therefore, the dinuclear cobalt(II) complexes having well-established structures are suitable candidates for investigating the magnetic interactions between the paramagnetic metal centers transmitted via different endogenous and/or exogenous bridging ligands.[34,35] However, it is still a labyrinth because not all the structures could be constructed as predicted, which might be ascribed to the different factors that control the formation of their molecular architectures.[36,37] The main challenge of building well-defined dinuclear complexes with expected geometric and electronic structures lies in the assembly of nuclearities induced by several factors, such as ligand-to-metal ratio, nature of the exogenous ancillary bridging groups, coordinating/noncoordinating ions, solvent systems, pH, temperature, etc.[38]

Cobalt and its related complexes have also numerous inhibitory effects on the bacterial cell, including the synthesis of polysaccharides, enhancement of bacterial cell membrane penetration, blocking of metal binding sites on enzymes, production of glucosyltransferase, cell membrane damage, etc.[39,40] Even though a large number of complexes of Zn(II), Cu(II), and Fe(III) showing antibacterial activities are reported in the literature,[41−45] a very few Co(II)-based complexes with antibacterial properties have been explored with mechanistic details.[46,47] A majority of reported studies on cobalt have exhibited antibacterial activities either in salt or nanoparticle forms.[48,49] There are also evidences that the adaptation capability of bacteria becomes enhanced in the presence of free Co(II) salt.[50] Consequently, the development of functionalized organo-chelated Co(II) complexes embodies a potential therapeutic approach for combating the growth of wide-ranging bacterial infections. This demand is further driven by an emerging medical problem of bacterial drug resistance to presently available commercial antibiotics.

Among the different bridging ligands explored, the carboxylate-based ligands appear very appealing because of their varied conformations, specifically *syn-syn*, *syn-anti,* and *anti-anti* that can lead to the formation of various di- and multinuclear complexes with novel topologies and interesting properties. In this context, the research and associated studies on carboxylate containing metal complexes as magnetic materials and therapeutic drugs are in continuous development.[51,52] In case of carboxylate-bridged high-spin cobalt(II) complexes, a very few examples with magneto-structural correlations are known where moderate antiferromagnetic interactions occur across the *syn-syn*[53] conformations and ferro−/antiferromagnetic interactions take place through *syn-anti*[54] and *anti-anti*[55] conformations. This versatility of the carboxylate group as a ligand has oriented its use to build an extended family of coordination complexes showing potential applications as magnetic materials.[56] Again, continuing our research on biological activities of metal complexes of carboxylate-based ligands, we have also reported anticancer, antidiabetic, antibiofilm, and glycosidase/phosphatase activities of iron(III), nickel(II), copper(II), and zinc(II) complexes.[52,57−60] The multidentate ligand, *N*,*N*′-bis[2-carboxybenzomethyl]-*N*,*N*′-bis[2-pyridylmethyl]-1,3-diaminopropan-2-ol (H_3cpdp) incorporating two benzoate and two pyridine functionalities, has been well-established in studying coordination complexes with diverse applications in biological activities and magnetic properties.[57−59,61−63] Therefore, motivated by our ongoing research interests in designing of smart scaffolds for exploration of magnetic and biological features in a synchronized manner, we extended our attention to synthesize a new family of high-spin cobalt(II) complexes. In the present contribution, we report the syntheses, X-ray crystal structures, variable temperature magnetic properties, and in vitro antibacterial activities of a series of high-spin

Scheme 1. Schematic Pathway for the Synthesis of Complexes 1−3

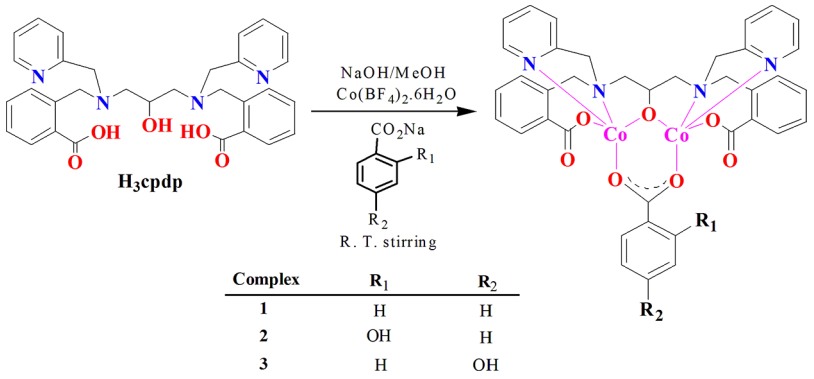

Complex	R_1	R_2
1	H	H
2	OH	H
3	H	OH

dinuclear cobalt(II) complexes $[Co_2(cpdp)(\mu\text{-}O_2CC_6H_5)]$ (**1**), $[Co_2(cpdp)(\mu\text{-}o\text{-}O_2CC_6H_4(OH))]\cdot H_2O$ (**2**), and $[Co_2(cpdp)(\mu\text{-}p\text{-}O_2CC_6H_4(OH))]\cdot 5H_2O$ (**3**).

RESULTS AND DISCUSSION

General Synthesis and Characteriz ation. Synthesis of dinuclear Co(II) complexes **1**−**3** under present investigation was achieved via successful utilization of carboxylate-affixed multidentate ligand, H_3cpdp. Originally, the H_3cpdp was synthesized and characterized following our previously published procedure.[58] It is pertinent to mention that the ligand H_3cpdp has two outstanding features which effectively support the formation of **1**−**3** by tuning the coordination modes: (i) it holds alkoxide-amine-carboxylate-based two symmetrical compartments as metal binding sites and (ii) the inner pendant alkoxide wing acts as the spacer-cum-bridging component between two cobalt centers, thus forming the self-assembled bridged-dicobalt(II) complexes with compact metal−metal cooperativity. As depicted in Chart 1, the alkoxide and carboxylate groups of H_3cpdp exhibit a number of coordination modes (A−F) during complexation with different metal ions. Among them, the coordination modes C, D, E, and F are very attractive resulting in the formation of Cu(II)- and Zn(II)-based tri-, tetra, hexa-, octa-, and decanuclear complexes with fascinating architectures.[57,62,64,65] In view of that, dinuclear Co(II) complexes **1**−**3** were synthesized following the routes outlined in Scheme 1. Indeed, complexes **1**−**3** were obtained directly by one-pot synthesis, starting from H_3cpdp and $Co(BF_4)_2\cdot 6H_2O$ in the presence of $C_6H_5CO_2Na$, $o\text{-}C_6H_4(OH)CO_2Na$ or $p\text{-}C_6H_4(OH)CO_2Na$ as ancillary ligands under ambient conditions.

As shown in Scheme 1, the reaction of $Co(BF_4)_2\cdot 6H_2O$ with H_3cpdp and $C_6H_5CO_2Na/o\text{-}C_6H_4(OH)CO_2Na/p\text{-}C_6H_4(OH)CO_2Na$ separately in 2:1:1 molar ratio in the presence of NaOH in methanol produced pink solution and allowed the subsequent isolation of well-shaped X-ray quality pink single crystals of $[Co_2(cpdp)(\mu\text{-}O_2CC_6H_5)]$ (**1**), $[Co_2(cpdp)(\mu\text{-}o\text{-}O_2CC_6H_4(OH))]\cdot H_2O$ (**2**), and $[Co_2(cpdp)(\mu\text{-}p\text{-}O_2CC_6H_4(OH))]\cdot 5H_2O$ (**3**) in good yield, by slow diffusion of diethyl ether into the clear filtrate. Use of NaOH facilitates the deprotonation of both the alcoholic and carboxylic groups of H_3cpdp. It is noteworthy to mention that the BF_4^-, Cl^-, and OAc^- ions normally act as counter anions. However, the Cl^- and OAc^- have strong binding ability with metal ions, thus sitting as either terminally coordinated or bridging coordinated inside the coordination sphere. On the other hand, the BF_4^- has very poor coordinating ability with metal ions, and hence, it can assemble mostly outside the coordination sphere. In the present investigation, we also tried to isolate and crystallize the $[Co^{II}_2]$ complexes of $cpdp^{3-}$ by utilizing $CoCl_2\cdot 6H_2O$ and $Co(OAc)_2\cdot 4H_2O$ salts; however, we did not succeed to crystallize them. In contrast, the use of $Co(BF_4)_2\cdot 6H_2O$ salt with $cpdp^{3-}$ in combination with stoichiometric amounts of $C_6H_5CO_2Na$, $o\text{-}C_6H_4(OH)CO_2Na$ and $p\text{-}C_6H_4(OH)CO_2Na$ separately facilitates the crystallization and subsequent isolation of the studied $[Co^{II}_2]$ complexes. In essence, the ancillary benzoate, *ortho*-hydroxybenzoate, and *para*-hydroxybenzoate ligands control the overall crystallization process through the bridging binding with two Co(II) ions in $\mu\text{:}\eta^1\text{:}\eta^1$-*syn-syn* bidentate manner. Complexes **1**−**3** were fully characterized by microanalysis, molar conductance, FTIR, UV−vis, electrospray ionization mass spectrometry (ESI-MS), powder X-ray diffraction (PXRD), and thermogravimetric analysis (TGA) techniques. X-ray structural analyses of **1**−**3** established their molecular frameworks.

In solution, the molar conductance data of metal complexes help to predict their conducting nature as well as the composition. Hence, we have performed the conductometric experiment for all three complexes in triplicate in MeOH solution at room temperature with a solute concentration of 10^{-3} M, and their data were recorded. The molar conductance values of 29, 21, and 19 Ω^{-1} cm^2 mol^{-1} for **1**, **2**, and **3**, respectively, are appreciably lower, suggesting their non-electrolytic nature.[66−69] The exogenous $C_6H_5CO_2^-$, $o\text{-}C_6H_4(OH)CO_2^-$, and $p\text{-}C_6H_4(OH)CO_2^-$ ions lying in the coordination sphere of **1**−**3** are bonded to cobalt(II) ions through bidentate bridging mode to satisfy the valences. The results obtained from the measurement of molar conductance are in agreement with their X-ray crystal structures.

FTIR and UV−vis Spectroscopy. In complexes **1**−**3**, two different coordination modes of carboxylates, namely, monodentate terminal and *syn-syn* bidentate bridging coordination of both the endogenous and exogenous benzoate groups have been established by the FTIR spectra (Figures S1−S3, Supporting Information). Deacon and Phillips have cautiously analyzed the FTIR spectra of several metal complexes that contain carboxylate groups having known single-crystal X-ray structures with constructive conclusions for the correlations between carboxylate stretching frequencies and their geometries.[70] The FTIR spectra of **1**−**3** show two strong stretching frequencies at 1605 and 1550 cm^{-1}, 1609 and 1557 cm^{-1}, and 1608 and 1541 cm^{-1} respectively, correspond-

ing to the two asymmetric vibration modes of benzoate groups. Similarly, two strong stretching frequencies at 1440 and 1406 cm^{-1}, 1467 and 1385 cm^{-1}, and 1445 and 1408 cm^{-1} respectively, correspond to the two symmetric vibration modes of benzoate groups. The differences between $\nu_{as}(COO^-)$ and $\nu_s(COO^-)$ stretches (Δ) of 199 and 110 cm^{-1} for **1**, 224 and 90 cm^{-1} for **2**, and 200 and 96 cm^{-1} for **3** which are the characteristic features of monodentate terminal and μ:η^1:η^1-*syn-syn* bidentate coordination of carboxylate groups, respectively, are in agreement with previous studies.[70−72] The band detected at higher stretching frequencies of 1605, 1609, and 1608 cm^{-1} for **1**, **2**, and **3** respectively, which can be attributed to ν(C═N) vibration of the pyridine moiety of the ligand backbone, is most probably overlapped with one of the asymmetric modes of benzoate groups. Furthermore, the characteristic stretching frequencies of 3420, 3416, and 3397 cm^{-1} for **1**, **2**, and **3**, respectively, are indicative of the noncoordinating hydroxyl ν(O−H) groups of lattice waters/moisture.[73]

The UV−vis spectra of **1**−**3** were recorded in methanol solution at room temperature (Figures S4−S6, Supporting Information). The spectra exhibit several low intense broad absorption bands at 560, 525, and 485 nm for **1**; 557, 527, and 483 nm for **2**; and 561, 522, and 482 nm for **3** which could be attributed to d-d transitions. In order of increasing energy, these bands may be identified as the $^4A_2'(^4F) \rightarrow {}^4E'(^4F)$,$^4A_2'(^4F) \rightarrow {}^4A_2'(^4P)$, and $^4A_2'(^4F) \rightarrow {}^4E''(^4P)$ transitions, respectively.[74] The d−d bands observed for **1**−**3** are more consistent with the distorted trigonal bipyramidal geometry, an assignment which is in agreement with the results obtained from single-crystal X-ray structure analyses.[75−77] All three complexes show Co(II)-bound ligand-based n → π^* and $\pi \rightarrow \pi^*$ transitions at 265 and 225 nm, 264 and 233 nm, and 255 and 213 nm for **1**, **2**, and **3**, respectively.[77,78] Hence, the experimental electronic spectra of the complexes justified the five-coordinate trigonal bipyramidal geometries around the Co(II) ions.[79,80]

Mass Spectrometry. In an effort to assess the identity of **1**−**3** in solution, ESI-MS was carried out using methanol solutions of the complexes. The ESI-MS of $[Co_2(cpdp)(\mu\text{-}O_2CC_6H_5)]$ (**1**), shown in Figure S7 of the Supporting Information, contains signals corresponding to $\{[Co_2(cpdp)(\mu\text{-}O_2CC_6H_5)] + Na\}^+$ at m/z = 799 (100%) as well as $\{[Co_2(cpdp)]\cdot 4CH_3OH\}^+$ at m/z = 783 (7%) and $\{[Co_2(cpdp)]\}^+$ at m/z = 655 (13%). Under the identical experimental conditions, the ESI-MS of $[Co_2(cpdp)(\mu\text{-}o\text{-}O_2CC_6H_4(OH))]\cdot H_2O$ (**2**), displayed in Figure S8 of the Supporting Information, shows signals corresponding to $\{[Co_2(cpdp)(\mu\text{-}o\text{-}O_2CC_6H_4(OH)) + Na\}^+$ at m/z = 815 (10%), $\{[Co_2(cpdp)]\cdot 4H_2O + OH + Na\}^+$ at m/z = 767 (100%) and $\{[Co_2(cpdp)]\}^+$ at m/z = 655 (42%). Similarly, the ESI-MS of $[Co_2(cpdp)(\mu\text{-}p\text{-}O_2CC_6H_4(OH))]\cdot 5H_2O$ (**3**) (Figure S9, Supporting Information) exhibits signals corresponding to $\{[Co_2(cpdp)(\mu\text{-}p\text{-}O_2CC_6H_4(OH)) + Na\}^+$ at m/z = 815 (100%) and $\{[Co_2(cpdp)]\}^+$ at m/z = 655 (38%). Therefore, the mass spectrometric studies of **1**−**3** suggest that the dinuclear identity of all three complexes with ancillary bridging benzoate/*ortho*-hydroxybenzoate/*para*-hydroxybenzoate group is retained in solution.

Description of Single-Crystal X-ray Structures of Complexes 1−3. X-ray diffraction analyses of the complexes were performed on appropriate single crystals at 273 K for **1** and 100 K for **2** and **3**. Complexes **1**−**3** crystallize in the monoclinic space group *C*2/*c*. The ORTEP views of the crystal structures of **1**−**3**, with labeling of selected atoms, are depicted in Figures 1, 2, and 3. Crystallographic data and refinement

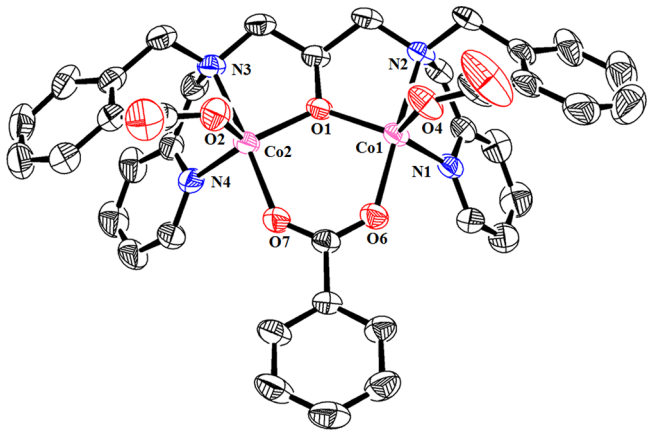

Figure 1. ORTEP view of the $[Co_2(cpdp)(\mu\text{-}O_2CC_6H_5)]$ unit of **1** having ellipsoids at 35% probability with a partial atom-numbering scheme. Hydrogen atoms and lattice waters are omitted for clarity. Color code: Co, pink; N, blue; O, red; C, black.

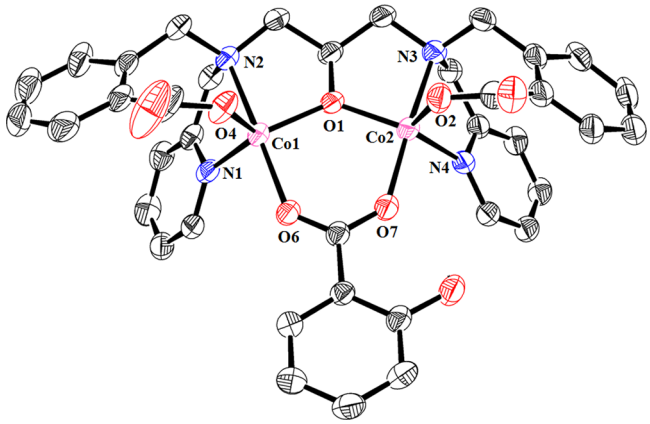

Figure 2. ORTEP view of the $[Co_2(cpdp)(\mu\text{-}o\text{-}O_2CC_6H_4(OH))]$ unit of **2** having ellipsoids at 35% probability with a partial atom-numbering scheme. Hydrogen atoms and lattice waters are omitted for clarity. Color code: Co, pink; N, blue; O, red; C, black.

parameters of **1**−**3** are summarized in Table 1. Selected bond distances and angles for **1**−**3** are summarized in Tables S1−S3 of the Supporting Information.

The structure of **1** contains a dinuclear $[Co_2(cpdp)(\mu\text{-}O_2CC_6H_5)]$ unit in its crystal lattice. The crystal structure of **2** consists of a dinuclear $[Co_2(cpdp)(\mu\text{-}o\text{-}O_2CC_6H_4(OH))]$ species, together with one molecule of lattice H_2O. Similarly, the structure of **3** comprises a dinuclear $[Co_2(cpdp)(\mu\text{-}p\text{-}O_2CC_6H_4(OH))]$ species, together with five H_2O molecules in the crystal lattice. All three complexes are isostructural, and their crystal structures simultaneously consist of a deprotonated ligand $cpdp^{3-}$ which acts as a μ-bis(tetradentate) ligand coordinated to two Co(II) ions. The two Co(II) ions are bridged and chelated by one $cpdp^{3-}$ ligand in their dinuclear $[Co_2]$ units where the exogenous $C_6H_5CO_2^-$ group in **1**, *o*-$C_6H_4(OH)CO_2^-$ group in **2**, and *p*-$C_6H_4(OH)CO_2^-$ group in **3** connect the two cobalt centers in a bidentate manner. Effectively, the two cobalt centers of the dinuclear unit of **1**, **2**, and **3** are crystallographically independent. In all three

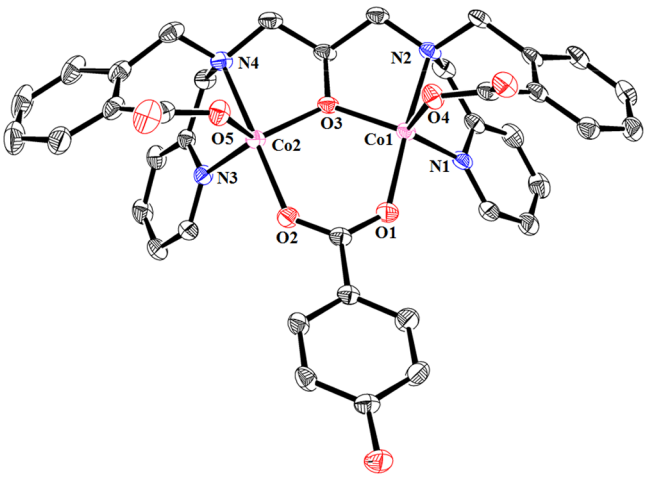

Figure 3. ORTEP view of the $[Co_2(cpdp)(\mu\text{-}p\text{-}O_2CC_6H_4(OH))]$ unit of **3** having ellipsoids at 35% probability with a partial atom-numbering scheme. Hydrogen atoms and lattice waters are omitted for clarity. Color code: Co, pink; N, blue; O, red; C, black.

structures, the cobalt centers lie in the distorted trigonal bipyramidal CoN_2O_3 environments, where each Co(II) is coordinated to one bridging alkoxide oxygen, one carboxylate oxygen, and one pyridine nitrogen of the $cpdp^{3-}$ ligand in equatorial positions. The axial positions are occupied by one tertiary amine nitrogen of the $cpdp^{3-}$ ligand and one exogenous carboxylate oxygen atom. The distortion of trigonal bipyramidal coordination geometry around the cobalt center is indicated by the value of trigonality factor, τ (Co1, 0.847 and Co2, 0.877 in **1**; Co1, 0.908 and Co2, 0.894 in **2**; Co1, 0.853 and Co2, 0.936 in **3**).[81] Comparable results concerning the changes in geometries in the vicinity of Co(II) ions in **1**−**3** have been accomplished by scrutinizing SHAPE analysis data (Table S4, Supporting Information).[82,83] In **1**, the deviations of the Co1 and Co2 centers from the O(1)O(4)N(1) and O(1)O(2)N(4) equatorial planes are detected as 0.220 and 0.211 Å, respectively. In **2**, the deviations of the Co1 and Co2 centers from the O(1)O(4)N(1) and O(1)O(2)N(4) equatorial planes are detected as 0.205 and 0.192 Å, respectively. Likewise, the Co1 and Co2 centers in **3** show deviations of 0.235 and 0.237 Å from the O(3)O(4)N(1) and O(3)O(5)N(3) equatorial planes, respectively.

In all three complexes, the average $Co-N_{axial}$ bond distances are significantly longer than the average $Co-N_{equatorial}$ bond distances ($Co-N_{axial}$, 2.187 Å and $Co-N_{equatorial}$, 2.058 Å in **1**; $Co-N_{axial}$, 2.166 Å and $Co-N_{equatorial}$, 2.061 Å in **2**; $Co-N_{axial}$, 2.182 Å and $Co-N_{equatorial}$, 2.057 Å in **3**). Similarly, the average $Co-O_{axial}$ bonds are notably longer than the $Co-O_{equatorial}$ bonds ($Co-O_{axial}$, 2.016 Å and $Co-O_{equatorial}$, 1.962 Å in **1**; $Co-O_{axial}$, 2.034 Å and $Co-O_{equatorial}$, 1.963 Å in **2**; $Co-O_{axial}$, 2.016 Å and $Co-O_{equatorial}$, 1.975 Å in **3**). Overall, the Co−O and Co−N bond distances are in good agreement with those of analogous dicobalt(II) complexes.[30,41,84−86] In all three complexes, the alkoxide bridge is close to symmetric with two $Co-O_{bridging\ alkoxide}$ bond distances differing about 0.004, 0.011, and 0.012 Å in **1**, **2**, and **3**, respectively. On the other hand, in all three complexes, the exogenous benzoate, *o*-hydroxy benzoate, and *p*-hydroxy benzoate groups bridge two Co(II) ions in μ:η^1:η^1-*syn-syn* bidentate mode, suggesting that this bridge is asymmetric (Co1−O6, 2.033(3) Å and Co2−O7, 2.000(3) Å in **1**; Co1−O6, 2.050(3) Å; Co2−O7, 2.019(3) Å in **2**; Co1−O1, 1.9962(14) Å, and Co(2)−O(2), 2.0369(14) Å in **3**). The $Co-O_{bridging\ alkoxide}-Co$ bond angles, spanning the alkoxide bridge, do vary significantly (123.1(1)−124.9(1)°). The sharp bridging angles exhibited by these complexes indicate the flexibility of $cpdp^{3-}$ ligand to hold two Co(II) ions in close proximity. As shown in Figure 4, the inter-metallic

Table 1. Single Crystal X-ray Data of $[Co_2(cpdp)(\mu\text{-}O_2CC_6H_5)]$ (1), $[Co_2(cpdp)(\mu\text{-}o\text{-}O_2CC_6H_4(OH))]\cdot H_2O$ (2) and $[Co_2(cpdp)(\mu\text{-}p\text{-}O_2CC_6H_4(OH))]\cdot 5H_2O$ (3)[a,b]

	1	2	3
empirical formula	$C_{38}H_{34}N_4O_7Co_2$	$C_{38}H_{36}N_4O_9Co_2$	$C_{38}H_{44}N_4O_{13}Co_2$
formula weight	776.58	810.59	882.63
crystal system	monoclinic	monoclinic	monoclinic
space group	*C*2/*c*	*C*2/*c*	*C*2/*c*
a, Å	20.7011(16)	20.4902(13)	20.5138(4)
b, Å	14.8718(12)	14.9772(10)	14.6452(3)
c, Å	27.243(2)	27.1562(17)	26.6686(4)
β, °	106.499(2)	106.443(3)	104.586(2)
volume, Å^3	8041.7(11)	7993.0(9)	7753.8(3)
Z	8	8	8
ρ, Mg/m^3	1.283	1.347	1.512
wavelength, Å	0.71073	1.54184	1.54184
temperature, K	273.15	100.00	100.00
F(000)	3207.882	3320.228	3664
μ, mm^{-1}	0.874	6.974	7.314
θ range, °	1.711 to 27.129	3.39 to 65.240	3.425 to 66.025
reflections collected	8870	6785	6743
independent reflections	5198	5971	6106
R(Fobsd data) [$I > 2\sigma(I)$]	0.0617	0.0653	0.0313
wR(F^2 all data)	0.1726	0.1792	0.0754
goodness-of-fit on F^2	1.0725	1.0416	1.0320
largest diff. peak and hole, e/Å^3	+0.6536 to −0.5550	+1.0112 to −0.6046	+0.302 to −0.340

[a] $wR_2 = \{\Sigma\,[w(F_o^2 - F_c^2)^2]/\Sigma\,[w(F_o^2)^2]\}^{1/2}$. [b] $R_1 = \Sigma||F_o| - |F_c||/\Sigma|F_o|$.

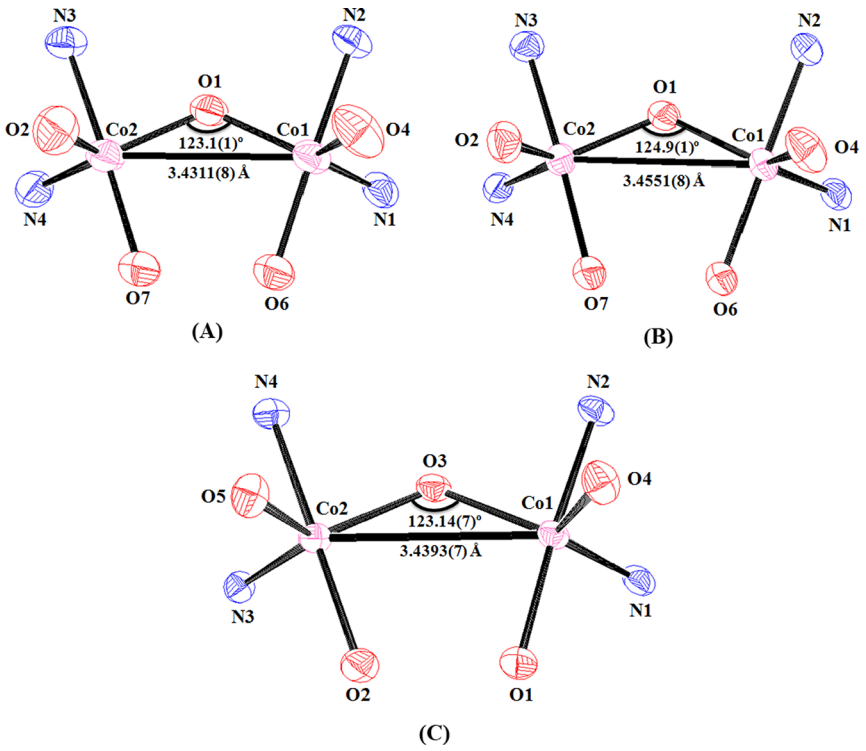

Figure 4. Views of core arrangements of (A) **1**; (B) **2**; and (C) **3** with cobalt−cobalt cooperativity.

Co···Co separations in **1**, **2** and **3** are 3.4311(8), 3.4551(8) and 3.4393(7) Å, respectively, which are comparable to those reported in the literature.[87−89]

The interesting features of the crystal structures of **1**−**3** lie in their supramolecular weak interactions. Complexes **2** and **3** exhibit mainly two sets of hydrogen bonding interactions in their crystal structures: (i) hydrogen bonding interaction (O−H···O) between the oxygen atom (donor) from lattice water and oxygen atom (acceptor) from lattice water; (ii) hydrogen bonding interaction (O−H···O) between the oxygen atom (donor) from lattice water and oxygen atom (acceptor) from the carboxylate oxygen atom. These hydrogen bonding interactions offer an extra stabilization to their crystal lattices. The unit cell packing diagrams of **2** and **3** showing hydrogen bonding interactions are illustrated in Figure S10 of the Supporting Information. It is also important to state that the crystal structure of **2** holds an additional intramolecular hydrogen bonding interaction at an O8−H8···O7 distance of 1.818 Å (O8···O7 = 2.554 Å) between the *o*-hydroxy oxygen atom (donor) and carboxylate oxygen atom (acceptor) which is expected further to stabilize its dimetallic bridging structure (Figure S11, Supporting Information). Moreover, the moderate intramolecular $\pi\cdots\pi$ stacking interactions observed in **1**−**3** also contribute toward the stabilization of the crystal lattices. Generally, in this type of interaction, the aromatic π-systems interrelate one another through their face-to-face arrangements, involving in a combination of dispersion and dipole-induced-dipole interactions.[90] In complexes **1**−**3**, the intramolecular $\pi\cdots\pi$ stacking interactions are observed because of the face-to-face arrangements of adjoining benzoate and pyridine rings with average centroid···centroid distances of 3.947, 3.958, and 3.900 Å, respectively (Figure S12, Supporting Information). These $\pi\cdots\pi$ stacking interactions observed in **1**−**3** are reasonable in magnitude when compared to the model porphyrin-porphyrin systems (3.4 Å).[91]

Description of Powder X-ray Diffraction (PXRD) Patterns of Complexes 1−3. PXRD experiments were performed using the microcrystalline samples of **1**−**3** isolated at pH 5.5 and 7.0. The PXRD patterns of **1**−**3** are illustrated in Figures S13−S15 of the Supporting Information. The experimental PXRD profiles of the bulk samples of **1**−**3** acquired at pH 5.5 and 7.0 exhibit more or less similar patterns without any significant difference, and they agree well with their simulated PXRD profiles. For all three complexes, the mercury software was applied to simulate the PXRD patterns from the atomic positions obtained from their single-crystal X-ray structures. These PXRD results authenticate the bulk purity of complexes **1**−**3** and their stability at physiological pH. However, there are very minute differences in the peak intensities in experimental and simulated patterns. The observed differences in the peak intensities are most possibly because of the selected orientation of applied power during carrying out the experiment.

Thermogravimetric Studies. Thermogravimetric analyses (TGA) of **1**−**3** were performed to examine their thermal stability. The TGA profiles illustrated in Figure S16 of the Supporting Information show two obvious mass losses for **1** and three mass losses for **2** and **3**. For **1**, the release of three CO_2 gas molecules in the first decomposition step occurs within 145−192 °C suggesting a mass loss of 17.36% (calcd. 17.00%). The second mass loss may be attributed to thermal decomposition of the metal−organic framework within 192−822 °C. For **2** and **3**, the removal of lattice waters (one lattice water for **1**; five lattice waters for **2**) takes place within 34−56 °C and 32−86 °C in the first decomposition step, showing a mass loss of 2.44% (calcd. 2.22%) and 10.13% (calcd. 10.21%), respectively. The second decomposition steps are associated with exclusion of three CO_2 gas molecules within 207−298 °C and 233−341 °C specifying a mass loss of 16.34% (calcd. 16.29%) and 15.14% (calcd. 14.96%) for **2** and **3**, respectively.

In the third decomposition step of **2** and **3**, the metal−organic framework undergoes thermal degradation within 298−814 °C and 341−803 °C, respectively. For all three complexes, the left over masses indicate the formation of cobalt(II) oxide as the most likely end product.[92,93]

Variable-Temperature Magnetic Studies. In order to explore the nature and extent of magnetic coupling between the two Co(II) ions in complexes **1**−**3**, variable-temperature (2−300 K) magnetic susceptibility measurements were performed under an externally applied magnetic field of 0.1 Tesla. The $\chi_M T$ *versus* T plots for **1**, **2**, and **3** are shown in Figures 5, 6, and 7 (χ_M is the magnetic susceptibility per mol of

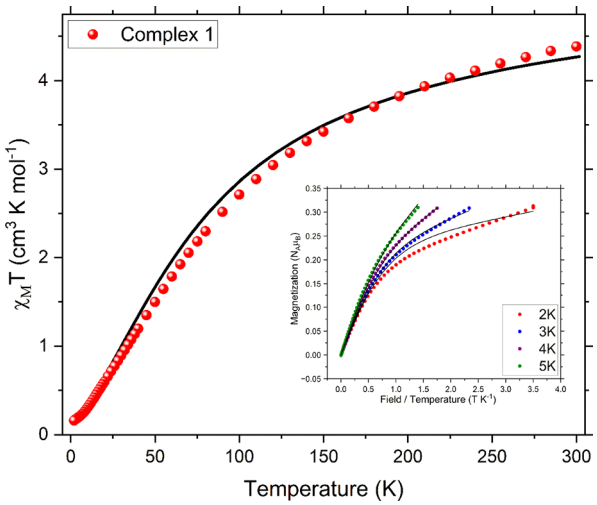

Figure 5. $\chi_M T$ vs T plot for **1**. (**Inset**) Reduced magnetization data (M vs H/T) for **1** collected under varying applied dc field. The solid line represents the best fit obtained with the isotropic exchange Hamiltonian.

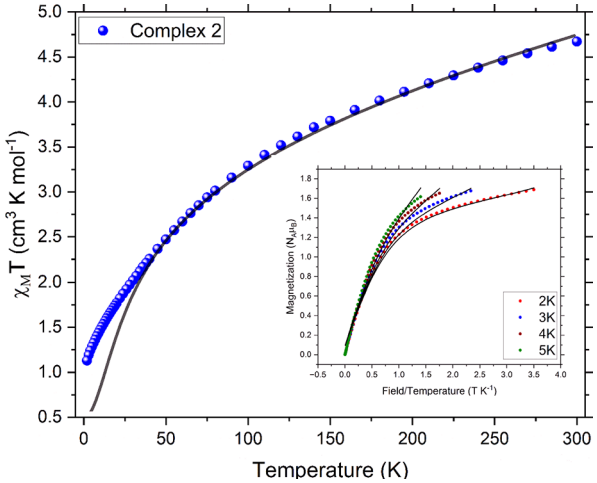

Figure 6. $\chi_M T$ vs T plot for **2**. (**Inset**) Reduced magnetization data (M vs H/T) for **2** collected under varying applied dc field. The solid line represents the best fit obtained with the isotropic exchange Hamiltonian.

the complex and T is the temperature). The values of $\chi_M T$ at 300 K are 4.45, 4.55, and 4.86 cm^3 K mol^{-1} for **1**, **2**, and **3**, respectively, which are quite larger than the spin-only value of 3.76 cm^3 K mol^{-1} expected for two noninteracting high-spin Co(II) ions with $S = {}^3/_2$ and $g = 2$. This phenomenon is due to the significant spin-orbit coupling effect for Co(II). On

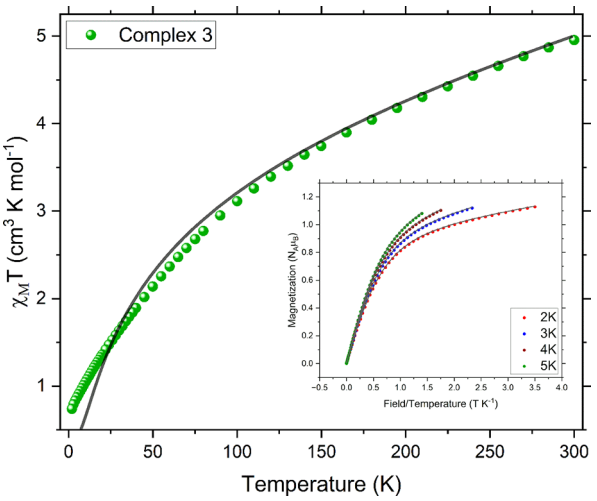

Figure 7. $\chi_M T$ vs T plot for **3**. (**Inset**) Reduced magnetization data (M vs H/T) for **3** collected under varying applied dc field. The solid line represents the best fit obtained with the isotropic exchange Hamiltonian.

lowering the temperature, the $\chi_M T$ values decrease gradually down to 100 K, and then decrease rapidly reaching the values of 0.20, 1.05, and 0.72 cm^3 K mol^{-1} at 2 K for **1**, **2**, and **3**, respectively. This behavior indicates the antiferromagnetic interactions between the two Co(II) ions. In the low-temperature regions, the final and rapid decrease of $\chi_M T$ values could be ascribed to the partial depopulation of excited magnetic states, zero-field splitting effect, and/or intermolecular interactions. Simultaneously to investigate the magnetic behavior of **1**−**3**, the measurements of field dependent magnetization (M vs H) were performed in the range of 0−7 Tesla at different temperatures of 2.0, 3.0, 4.0, and 5.0 K. Insets of Figures 5−7 display the M/Nμ_B vs H/T plots. It was observed that the magnetization values for all three complexes increase rapidly with increasing the magnetic field in the low-field and low-temperature regions. The magnetization value for **1** is 0.33 Nμ_B which is significantly lower than the magnetization values of 1.70 Nμ_B for **2** and 1.12 Nμ_B for **3** at 2 K under 3.5 Tesla. The observed difference in magnetization for **1** from **2** and **3** may be attributed to values of J_x and J_y which are more or less similar for **2** and **3** (Table 2). The AC magnetic susceptibility measurements on **1**−**3** exclude any single molecule magnetic behavior.

A spin Hamiltonian eq 1 as shown below was used to fit the $\chi_M T$ vs T, and magnetization plots:

$$H = g\cdot\mu_B\cdot S\cdot B + D[S_z^2 - S(S+1)/3] + E(S_x^2 - S_y^2) - 2J\cdot S_1\cdot S_2 \quad (1)$$

where D and E represent the single-ion axial and rhombic zero-field splitting parameters. Ab initio CASSCF calculations[94] were also carried out by utilizing the MOLCAS package to evaluate the values of crystal field splitting parameters and g-tensors of individual ions in **1**−**3** (Table 2). These parameters obtained were used satisfactorily to find the values of exchange coupling constants using the software PHI.[95] The best fit between the experimental and simulated data was obtained with $J_x = J_y = -9.5$ cm^{-1}, $J_z = -25.9$ cm^{-1} and $g_x = 2.342$, $g_y = 2.276$, $g_z = 2.208$ for **1**; $J_x = J_y - 2.3$ cm^{-1}, $J_z = -44.3$ cm^{-1} and $g_x = 2.274$, $g_y = 2.278$, $g_z = 2.284$ for **2**; and $J_x = J_y = -3.2$ cm^{-1}, $J_z = -30.6$ cm^{-1} and $g_x = 2.316$, $g_y = 2.297$, $g_z = 2.224$ for **3**

Table 2. Crystal Field Splitting Parameters, *g*-Tensors, and Coupling Constants for 1−3

complex	D (cm^{-1})	E (cm^{-1})	g_x	g_y	g_z	J_x (cm^{-1})	J_y (cm^{-1})	J_z (cm^{-1})
1	13.130	−3.360	2.342	2.276	2.208	−9.5	−9.5	−25.9
2	14.791	−2.778	2.274	2.278	2.284	−2.3	−2.3	−44.3
3	10.088	−0.986	2.316	2.297	2.224	−3.2	−3.2	−30.6

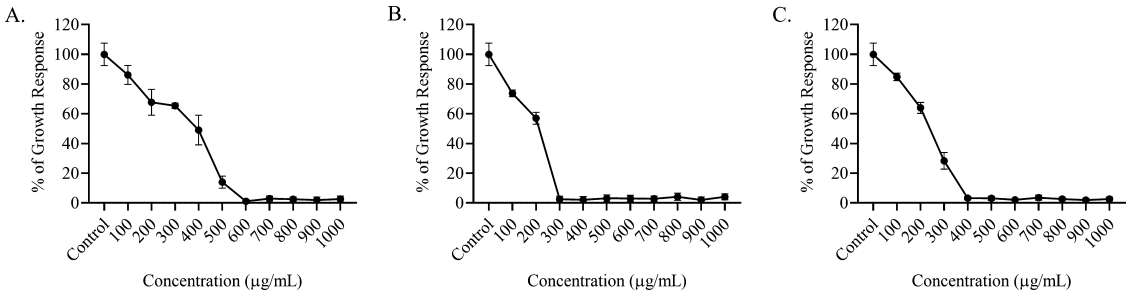

Figure 8. Determination of the MIC of complexes **1** (A), **2** (B), and **3** (C) on the growth of *Staphylococcus aureus*, SA96. MIC values of **1**−**3** were found to be 600, 300, and 400 μg/mL, respectively. Error bars indicate the mean of three replicates with ± SD.

(Table 2). The crystal field splitting parameters and *g*-tensors are comparable with the obtained *J* values which are plausible for five-coordinate Co(II) complexes.[96]

Furthermore, the reciprocals of magnetic susceptibilities ($1/\chi_M$) of the complexes were fitted quite satisfactorily by the Curie−Weiss law ($\chi_M = C/(T - \theta)$) over the specified temperature range, yielding the Weiss constants (θ) of −0.602, −0.702, and −1.870 K for **1**, **2**, and **3**, respectively. The plots of reciprocals of magnetic susceptibility vs temperature of **1**−**3** are shown in Figure S17 of the Supporting Information. The negative values of θ further confirmed the occurrence of antiferromagnetic interactions between the Co(II) ions and the associated spin-orbit coupling effect.

Careful literature search shows that alkoxide-bridged di- or multinuclear Co(II) complexes are very less common, and only a small number of structurally and magnetically characterized μ-alkoxide-bridged dinuclear Co(II) complexes are reported[97] in comparison to μ-phenoxide-bridged dinuclear cobalt(II) complexes.[98] Generally, the magnetic coupling can be affected by several structural parameters, such as the M-O-M bridging angle (α), the hinge distortion parameter (γ), and M···M internuclear separation. However, there is no unambiguous relationship between α and γ for μ-alkoxide-bridged [Co^{II}_2] complexes as reported earlier.[99] Therefore, a magneto-structural correlation can now be warranted considering the following structural features: (i) generally, it is believed that the ligand that bridges via a single atom controls the intercession of magnetic exchange; (ii) the nature of the exogenous ancillary bridging ligand plays an important role in mediating the magnetic interaction because it affects the bond strength between the metal ion and bridging ligand; (iii) in the metal complexes with bridging alkoxide oxygen atom where the primary interaction occurs through *p*-orbitals, the Co−$O_{bridging\ alkoxide}$−Co angle is very important since the value of the coupling constant (*J*) varies with variation of this angle. The latter statement offers a more rational justification for the coupling constants obtained with Co−$O_{bridging\ alkoxide}$−Co angles of 123.1(1), 124.9(1), and 123.14(7)° in **1**, **2**, and **3** respectively, which are in agreement with the earlier studies.[97−99] The equatorially coordinated bridging alkoxide oxygen atoms (Co−O_{equiv} = 1.943(3)−2.010(14) Å) in the trigonal bipyramidal CoO_3N_2 coordination geometry are closer than the axially coordinated bridging benzoate/*ortho*-hydroxybenzoate/*para*-hydroxybenzoate oxygen atoms (Co−O_{ax} = 1.996(14)−2.050(3) Å); thus, the equatorially oriented Co(II) orbital is magnetic in nature, while the axially oriented Co(II) orbital is not. It is also worth-mentioning that a larger M−O−M bridging angle (α) favors the strong antiferromagnetic interactions. In the present investigation, **1**−**3** represent a new family of dinuclear high-spin Co(II) complexes that contain one μ-alkoxide and one $\mu:\eta^1:\eta^1$-benzoate/*ortho*-hydroxybenzoate/*para*-hydroxybenzoate bridges where the magnitude of magnetic exchange is a linear function of the Co−O−Co bridging angle; in general, the exchange is antiferromagnetic for $\alpha > 97°$ and ferromagnetic for $\alpha < 97°$.[99] However, it should also be noted that the magnitude of magnetic exchange of the exchange-coupled Co(II) dimers at low temperature can be established not only by the strength of the exchange interaction but also by the type and extent of symmetry distortions around each interacting ion. As a result, complexes with similar Co−O−Co bridging bond angles sometimes can demonstrate different exchange interaction values and different magnetization behavior. In addition, the ancillary bridging functionalities, i.e., benzoate, *ortho*-hydroxybenzoate, and *para*-hydroxybenzoate may have an impact on cobalt−cobalt cooperativity, an important structural parameter for magnetic exchange. Therefore, in the present study, the different exchange interaction values, though quite small, may be justified in spite of having similar Co−O−Co bridging angles.

Investigation of Antibacterial Activity of Complexes 1−3: Determination of Minimum Inhibitory Concentrations (MICs). All three model complexes were evaluated for antibacterial activity against *Staphylococcus aureus*, SA96 with an enhanced percent activity index as compared to free ligands such as H_3cpdp, $C_6H_5CO_2Na$, *o*-$C_6H_4(OH)CO_2Na$, and *p*-$C_6H_4(OH)CO_2Na$ alone. In order to investigate the antibacterial activity, we determined the MIC values of the complexes, and these were observed to be 600, 300, and 400 μg/mL for **1**, **2**, and **3**, respectively (Figure 8). Supplementary data obtained from the treatment by utilizing free H_3cpdp, $C_6H_5CO_2Na$, *o*-$C_6H_4(OH)CO_2Na$, and *p*-$C_6H_4(OH)CO_2Na$ alone showed no or very insignificant antibacterial activity (Figures S18 and S19, Supporting Information). Therefore, we used the MIC and 1/2 MIC values of complexes **1**−**3** for the rest of the biological experiments.

Effect of Complexes 1−3 on the Bacterial Growth by Crystal Violet (CV) Staining. CV assays were carried out to examine the effect of complexes **1**−**3** toward the inhibition of growth of *Staphylococcus aureus*, SA96. The results acquired from CV assay showed a considerable decrease in the bacterial population (Figure 9). It was also observed that the bacterial

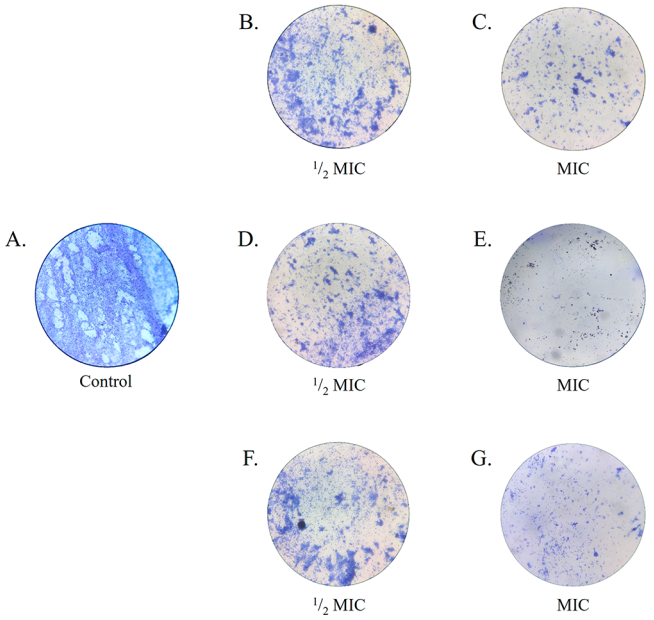

Figure 9. Light microscopic analysis showing the effect of complexes **1**−**3** on *Staphylococcus aureus*, SA96 with their increasing doses. (**A**) control set; (**B**) and (**C**) complex **1**-treated sets; (**D**) and (**E**) complex **2**-treated sets; (**F**) and (**G**) complex **3**-treated sets.

growth was inhibited by the complexes in a concentration-dependent manner, suggesting that the growth was inhibited more effectively at their MIC doses compared to that at 1/2 MIC doses. The CV assay also specified that **2** and **3** were found to be more efficient in inhibiting the bacterial growth in comparison to **1** both at MIC and 1/2 MIC doses. Figure 9A shows the control set where only 1% (v/v) DMSO was used instead of any cobalt complex.

Effect of Complexes 1−3 on the Bacterial Cell Membrane by Assessing the Cellular Leakage. In order to gain insight into the possible mechanistic aspect, the bacterial cell membrane degradation was examined by measuring the cellular leakage of DNA. In view of that, the DNA leakage experiment on *Staphylococcus aureus*, SA96 was conducted by measuring the absorbance at λ_{max} = 260 nm.[100] The permeabilized membrane permits the leakage of nucleic acids like DNA, and hence, it would be a good facet to take into consideration while confirming the membrane damage. When the cells of *Staphylococcus aureus*, SA96, were treated with MIC and 1/2 MIC doses of **1**−**3**, the spectrophotometric data showed the absorbances that were increased appreciably in a dose- and time-dependent manner of the complexes in comparison to untreated cells (Figure 10). The results also suggested that the antibacterial activity of complexes **1**−**3** originated through the damage of the bacterial cell membrane.

Investigation of the Combinatorial Effect of Complexes 1−3 with Gentamicin against *Staphylococcus aureus*, SA96. A combinatorial study was performed to gain insight into the synergistic effect of each of the model complexes with gentamicin against *Staphylococcus aureus*, SA96. Gentamicin belongs to the class of aminoglycoside-based antibiotics that work by killing bacteria or preventing their growth. As determined, the MIC value of gentamicin is 0.5 μg/mL against *Staphylococcus aureus*, SA96 (Figure S20, Supporting Information). It was observed that the combination of gentamicin with complexes **1**, **2**, and **3** separately exhibited better inhibition to the growth of *Staphylococcus aureus*, SA96 in comparison to individual therapy (Figure S21, Supporting Information). As displayed in Figure S21 of the Supporting Information, complexes **1**, **2**, and **3** could kill the maximum number of bacterial cells of 94.63, 97.29, and 98.33% respectively, at their 1/2 MIC values in combination with 1/2 MIC of gentamicin.

Comparison of Antimicrobial Activities of Complexes 1−3. Usually, the metal complexes have a stronger antibacterial activity compared to their noncomplexed organic counterparts or ligands. It is well established that the ligands and related metal complexes play a significant role in the bactericidal activity of the compounds.[101] The chelation of organic ligands with suitable metal ions enhances their bioavailability and bioactivity. The chelation process also increases electron polarization around the chelate ring, permeation into the lipid membranes, and subsequent hindrance to the metal absorption sites in microorganisms. In the present investigation, the design strategy is based on the complexation of Co(II) with carboxylate-affixed multidentate ligand H_3cpdp that was hypothesized to act as antibacterial agents. Complexes **1**−**3** have similar structural topologies except the exogenous bridging benzoates (benzoate for **1**; *ortho*-hydroxy benzoate for **2**; *para*-hydroxy benzoate for **3**) which offer added stabilization to the dimetallic [Co_2] cores.

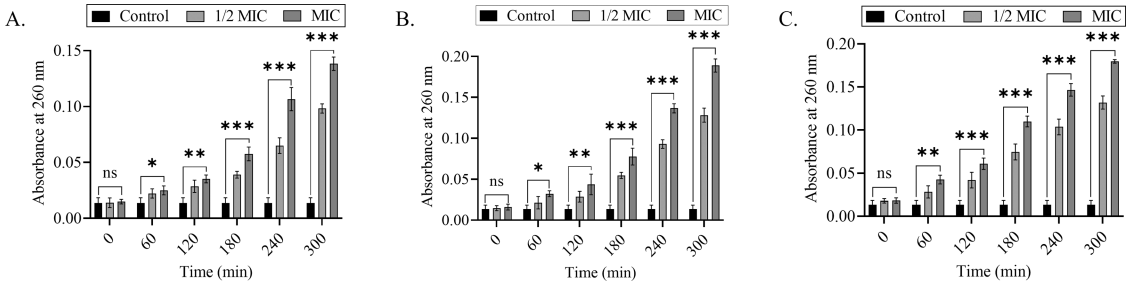

Figure 10. Mechanistic aspect of antibacterial activities of **1**−**3** against *Staphylococcus aureus*, SA96 by determining DNA leakage after administration of MIC and 1/2 MIC doses of **1** (A), **2** (B), and **3** (C), and 1% (v/v) DMSO as a control. The leakage of DNA as a measure of absorbance at 260 nm was plotted against different time points (0−300 min). Error bars indicate the mean of three replicates with ± SD, where ns = $P > 0.05$, * = $P < 0.05$, ** = $P < 0.01$, *** = $P < 0.001$, compared with the control.

All three complexes conserve their dimetallic identity in solution as evidenced by molar conductance, UV−vis spectroscopic, and mass spectrometric data and showed potential antibacterial activities. Hence, we have compared the antibacterial activities of **1**−**3** by rationalizing their MIC values. The comparative assessment of their antibacterial activities indicated that the overall order of their effectiveness against *Staphylococcus aureus*, SA96 was recorded as follows: **2** > **3** > **1**. The different activities of **1**−**3** are most possibly due to the presence of the different exogenous benzoate groups coordinated to Co(II) ions and different degree of distortion of coordination geometries. Among the three exogenous bridging benzoate groups, *ortho*-hydroxy benzoate is weakly acidic and *para*-hydroxy benzoate is little-bit more acidic, whereas unsubstituted benzoate is weakly basic in nature. Bacteria frequently encounter difficulties to survive in weakly acidic conditions.[102] However, the antibacterial mode of action of weakly acidic compounds is not fully understood. It is typically agreed that the ability of weakly acidic compounds to inhibit bacterial growth is linked to their lipid permeability.[103] In **2** and **3**, the presence of *ortho*-hydroxybenzoate and *para*-hydroxybenzoate groups makes them weakly acidic, thereby facilitating the inhibition of bacterial growth and increasing their effectiveness in comparison to **1**. Nevertheless, no obvious benefits of bridging benzoate/substituted benzoate moieties could be obtained at this stage. To better understand the detailed mechanistic aspects underlying the antibacterial activities of model cobalt complexes **1**−**3**, further studies will be necessary. When compared with literature reports, the MIC values obtained for the complexes under current investigation are comparable to the values of allied Co(II) complexes.[104,105] Our results suggest that **1**−**3** are new additions to the important family of high-spin Co(II)-based antibacterial complexes.

CONCLUSIONS

In conclusion, this study represents the synthesis, crystal structures, variable-temperature magnetic studies, and antibacterial properties of a new family of μ-alkoxide-bridged high-spin $[Co^{II}_2]$ complexes $[Co_2(cpdp)(\mu\text{-}O_2CC_6H_5)]$ (**1**), $[Co_2(cpdp)(\mu\text{-}o\text{-}O_2CC_6H_4(OH))]\cdot H_2O$ (**2**), and $[Co_2(cpdp)(\mu\text{-}p\text{-}O_2CC_6H_4(OH))]\cdot 5H_2O$ (**3**) based on a multidentate ligand (H_3cpdp), in combination with benzoate/*ortho*-hydroxybenzoate/*para*-hydroxybenzoate groups. In comparison to the μ-phenoxide-bridged dicobalt(II) complexes reported in the literature, the μ-alkoxide-bridged dicobalt(II) complexes are uncommon, and only a very limited number of structurally and magnetically characterized μ-alkoxide-bridged $[Co^{II}_2]$ complexes are investigated previously. The ancillary benzoate, *ortho*-hydroxybenzoate, and *para*-hydroxybenzoate scaffolds are successfully utilized as bridging ligands for selective tuning of the ligand field strength around the cobalt(II) ions. In all three complexes, the benzoate/*ortho*-hydroxybenzoate/*para*-hydroxybenzoate group bridges two cobalt centers in a μ:η^1:η^1-*syn*-*syn* bidentate mode. These complexes can be isolated in the solid state, and they retain their divalent oxidation states in solution for an extend period of time. In each complex, cobalt centers exhibit distorted trigonal bipyramidal geometry as confirmed by single-crystal X-ray investigation and computational SHAPE analysis. The sharp $Co(II)-O_{bridging\ alkoxide}-Co(II)$ angles of values 123.1(1), 124.9(1) and 123.14(7)° exhibited by **1**, **2** and **3** indicate the flexibility of ligand $cpdp^{3-}$ to accommodate two Co(II) ions in close proximity, with intermetallic Co···Co separations of 3.4311(8), 3.454(1), and 3.4393(7) Å, respectively. The cobalt(II) ions in **1**−**3** are in a high-spin state over the temperature range of 2−300 K, showing moderate antiferromagnetic interactions among the cobalt centers. Elementary correlations of these complexes with some other related dicobalt(II) systems for which data are accessible suggest that the antiferromagnetic coupling, albeit moderate, is dependent significantly on the $Co(II)-O_{bridging\ alkoxide}-Co(II)$ angle than on the spatial Co···Co separations. The *in vitro* antibacterial activities of the free ligand H_3cpdp and its cobalt(II) complexes were evaluated against *Staphylococcus aureus*, SA96, indicating that the complexes exhibited improved activities against the bacterial strain than the free ligand. However, a comparative assessment of their antibacterial activities revealed that **2** and **3** showed higher activity compared to that of **1**, with MIC values of 600, 300, and 400 μg/mL for **1**, **2** and **3**, respectively. Our investigation also showed that the combinatorial application of complexes **1**−**3** with commercially available antibiotic, gentamicin can efficiently kill the *Staphylococcus aureus*, SA96 strain rather than its individual therapy.

EXPERIMENTAL SECTION

Reagents and Solvents. Coba lt(II) tetra fluorobora tehexahydrate, lithium hydroxide, 1,3-diamino-2-propanol, 2-carboxybenzaldehyde, and 2-picolylchloride hydrochloride were purchased from Sigma-Aldrich, Germany. The other reagents such as NaOH, $NaBH_4$, $C_6H_5CO_2Na$, o-$C_6H_4(OH)CO_2Na$ and p-$C_6H_4(OH)CO_2Na$, agar powder, and glycerol were purchased from Merck, India. Luria-Bertani (LB) broth was purchased from Himedia, USA. Mueller−Hinton (MH) broth, crystal violet (CV), and gentamicin were procured from SRL, India. All other chemicals and reagents were of analytical grade and obtained from Sigma-Aldrich, Germany and Himedia, USA. Water used in all the experiments executed in this work was prepared using a Milli-Q water purification system purchased from Millipore (Milford, MA, USA). All other materials were of reagent grade obtained from commercial sources and used without further purification. All other solvents used were of HPLC grade.

Synthesis of *N,N′*-Bis[2-carboxybenzomethyl]-*N,N′*-bis[2-pyridylmethyl]-1,3-diaminopropan-2-ol, H_3cpdp. The synthesis of ligand H_3cpdp was accomplished following our reported procedure.[58] The identity and composition of the ligand were authenticated by elemental analysis, FTIR, and NMR spectroscopy as well as mass spectrometry and thermogravimetric analysis. Yield: 4.018 g (77%).

Synthesis of $[Co_2(cpdp)(\mu\text{-}O_2CC_6H_5)]$ (1). $Co(BF_4)_2\cdot 6H_2O$ (0.313 g, 0.92 mmol) in MeOH (10 mL) was added drop wise to a stirred mixture in MeOH (10 mL) containing H_3cpdp (0.511 g, 0.46 mmol) and NaOH (0.055 g, 1.38 mmol). The mixture was stirred for 15 min resulting in a pink solution. Afterward, $C_6H_5CO_2Na$ (0.066 g, 0.46 mmol) in MeOH (2 mL) was slowly added to this solution, and the stirring was maintained for another 1 h. Then, the solution was filtered. The X-ray diffraction quality pink single crystals were obtained by diffusing diethyl ether into the clear filtrate after ∼7 days. Then, the product was filtered, washed with water, and dried under vacuum over anhydrous P_2O_5 in a desiccator. Yield: 0.272 g (75%). Anal. Calcd. for $C_{38}H_{34}N_4O_7Co_2$: C, 58.77%; H, 4.41%; N, 7.21%; Co, 15.18%. Found: C, 58.59%; H, 4.28%; N, 7.33%; Co, 15.34%. Molar conductance, Λ_M (MeOH) = 29 Ω^{-1} cm^2 mol^{-1}. FTIR (cm^{-1}): ν = 3420(b), 3068(b), 1605(s), 1550(s), 1484(s), 1440(s), 1406(s), 1295(s), 1155(s), 1119(s), 1104(s), 1028(s), 983(s), 938(s), 888(s), 864(s), 811(s), 761(s), 717(s), 683(s), 581(s), 554(s). UV−vis (MeOH): $\lambda_{max,nm}$ (ε, M^{-1} cm^{-1}) = 560 (146), 523 (128), 486 (114), 265 (13108), 225 (46368). Mass spectrum (ESI): m/z 799 (M^+ =

{[Co_2(cpdp)(μ-$O_2CC_6H_5$)] + Na}$^+$), 783 (M^+ = {[Co_2(cpdp)]·4CH_3OH}$^+$), 655 (M^+ = {[Co_2(cpdp)]}$^+$).

Synthesis of [Co_2(cpdp)(μ-*o*-$O_2CC_6H_4$(OH))]·H_2O (2). This compound was synthesized by employing the above procedure using H_3cpdp (0.511 g, 0.46 mmol), $Co(BF_4)_2$·$6H_2O$ (0.313 g, 0.92 mmol), NaOH (0.055 g, 1.38 mmol), and *o*-C_6H_4(OH)CO_2Na (0.074 g, 0.46 mmol). X-ray diffraction quality pink single crystals were obtained by diffusing diethyl ether into the clear filtrate after ∼5 days. Finally, the product was filtered, washed with water, and dried under vacuum over anhydrous P_2O_5 in a desiccator. Yield: 0.310 g (82%). Anal. Calcd. for $C_{38}H_{36}N_4O_9Co_2$: C, 56.31%; H, 4.48%; N, 6.91%; Co, 14.54%. Found: C, 56.49%; H, 4.34%; N, 6.84%; Co, 14.69%. Molar conductance, Λ_M (MeOH) = 21 Ω^{-1} cm^2 mol^{-1}. FTIR (cm^{-1}): ν = 3416(b), 1609(s), 1557(s), 1467(s), 1385(s), 1352(s), 1245(s), 1152(s), 1104(s), 1032(s), 985(s), 864(s), 811(s), 760(s), 688(s), 580(s). UV−vis (MeOH): $\lambda_{max,nm}$ (ε, M^{-1} cm^{-1}) = 557 (106), 527 (100), 483 (90), 264 (13800), 233 (35280). Mass spectrum (ESI): *m*/*z* 815 (M^+ = {[Co_2(cpdp)(μ-*o*-$O_2CC_6H_4$(OH)) + Na}$^+$), 767 (M^+ = {[Co_2(cpdp)]·4H_2O + OH + Na}$^+$), 655 (M^+ = {[Co_2(cpdp)]}$^+$).

Synthesis of [Co_2(cpdp)(μ-*p*-$O_2CC_6H_4$(OH))]·5H_2O (3). This compound was synthesized by employing the above procedure using H_3cpdp (0.511 g, 0.46 mmol), $Co(BF_4)_2$·$6H_2O$ (0.313 g, 0.92 mmol), NaOH (0.055 g, 1.38 mmol) and *p*-C_6H_4(OH)CO_2Na (0.074 g, 0.46 mmol). X-ray diffraction quality pink single crystals were obtained by diffusing diethyl ether into the clear filtrate after ∼7 days. Finally, the product was filtered, washed with water, and dried under vacuum over anhydrous P_2O_5 in a desiccator. Yield: 0.349 g (85%). Anal. Calcd. for $C_{38}H_{44}N_4O_{13}Co_2$: C, 51.71%; H, 5.02%; N, 6.35%; Co, 13.35%. Found: C, 51.66%; H, 5.12%; N, 6.27%; Co, 13.47%. Molar conductance, Λ_M (MeOH) = 19 Ω^{-1} cm^2 mol^{-1}. FTIR (cm^{-1}): ν = 3397(b), 1608(s), 1541(s), 1481(s), 1445(s), 1408(s), 1318(s), 1283(s), 1242(s), 1155(s), 1101(s), 1036(s), 927(s), 855(s), 763(s), 688(s), 618(s), 548(s), 504(s). UV−vis (MeOH): $\lambda_{max,nm}$ (ε, M^{-1} cm^{-1}) = 561 (202), 522 (175), 482 (114), 255 (27534), 213 (34015). Mass spectrum (ESI): *m*/*z* 815 (M^+ = {[Co_2(cpdp)(μ-*p*-$O_2CC_6H_4$(OH)) + Na}$^+$), 655 (M^+ = {[Co_2(cpdp)]}$^+$).

General Instrumental Methods. Microanalyses (C,H,N) were done by a PerkinElmer 2400 CHNS/O Series II elemental analyzer. The % of Cl^- and Br^- contents in the ligand H_3cpdp were obtained by potentiometric titration using $AgNO_3$ in aqueous solution with a Mettler Toledo Seven Compact S220 digital Ion/pH meter. The % of cobalt contents in complexes **1**−**3** were analyzed by the complexometric titration method using Na_2H_2EDTA, in aqueous solution, after digesting their crystalline powder samples in conc. HCl/HNO_3 mixture. The NMR spectra were recorded on a Bruker AC 400 NMR spectrophotometer. Fourier Transform infrared spectra were acquired by using KBr pellets on a PerkinElmer L120-000A spectrophotometer. The electronic spectra were measured at room temperature on a Shimadzu UV 1800 spectrophotometer. Mass spectra of cobalt complexes were obtained on a Micromass Q-Tof Micro (Waters) mass spectrometer. Powder X-ray diffraction patterns of **1**−**3** were obtained on a Rigaku (Mini Flex II) table-top X-ray diffractometer (Cu Kα = 1.54059 Å) with Bragg angular range, i.e., 2θ (5° < 2θ < 50°) using a silicon wafer sample holder at room temperature. The magnetic susceptibility data of **1**−**3** were collected on a MPMS-XL 5 T superconducting quantum interference device (SQUID) from Quantum Design using crystalline powder samples in the temperature range of 2−300 K under an external magnetic field of 0.1*T*. The powder samples were incorporated into the capsule with straw as the sample holder. Experimental susceptibility data were corrected for the underlying diamagnetism using Pascal's constant.[106] The temperature-dependent magnetic contribution of the holder was determined experimentally and subtracted from the measured susceptibility data. Spin Hamiltonian simulations of the data were achieved by applying the program PHI.[95] TGA was carried out by employing a NETZSCH STA 449F3 thermal analyzer. SHAPE analysis of the Co(II) coordination sphere in **1**−**3** was performed by using SHAPE software.[107] The value of Continuous Shape Measure (CShM) effectively indicates the best possible geometry.

Single-Crystal X-ray Structure Determination of 1−3. X-ray diffraction intensity data for **1** and **2** were collected on a Bruker SMART CCD diffractometer using a graphite-monochromated Mo Kα radiation (λ = 0.71073 Å), and for **3**, those were collected on a SuperNova, Dual, Cu at zero CCD diffractometer (λ = 1.54184 Å), both with a microfocus source and focusing multilayer mirror optics. Using the SAINT[108] package and SADABS[109] program, the processing of the crystallographic data and their absorption corrections were accomplished, respectively. All three structures were solved by direct methods using the program SIR-97[110] and refined anisotropically by full-matrix least-squares on F^2 with SHELXL,[111,112] including the OLEX2 program.[113] The difference Fourier map was used to position the hydrogen atoms. Consequently, the hydrogen atoms were located at calculated positions (C−H, 0.96 Å) and included in the structure calculation without further refinement of the parameters. The hydroxyl hydrogen atoms were located precisely.

Bacterial Strain and Culture Conditions. The gram-positive bacterial strain *Staphylococcus aureus*, SA96 was obtained from Microbial Type Culture Collection and Gene Bank (MTCC) and used in this study. The stock culture was grown for ∼18 h and then preserved in Luria−Bertani (LB) broth containing 20% (v/v) glycerol at −80 °C. Afterward, the frozen culture was revived from −80 °C by plating on an LB agar plate. Before carrying out each experiment, a single pure colony was inoculated into freshly prepared LB broth and incubated overnight at 37 °C under stirring conditions (200 rpm).

Study of Antibacterial Activity of Complexes 1−3: Determination of MICs. The MIC values of complexes **1**−**3** were established against *Staphylococcus aureus*, SA96 by employing microdilution technique of standard laboratory guidelines provided by Clinical and Laboratory Standards Institute (CLSI).[114] Actually, ∼5 × 10^5 CFU/mL cells were made from 18 h grown culture by using 0.5 McFarland standard solution and inoculated into 200 μL of Mueller Hinton (MH) broth with varying concentrations of **1**−**3** ranging from 100 to 1000 μg/mL in a sterile 96-well microtiter plate. A vehicle control (positive control) set was made with 1% DMSO (v/v) and the same volume of bacterial inoculum in the media in the absence of any cobalt complex. The sample plates were incubated at 37 °C for 24 h. The % of growth responses were measured by assessing the absorbance (OD) value at 595 nm in a microplate absorbance reader (iMark Microplate Absorbance Reader, Bio-Rad Laboratories). The MIC values were determined as the minimum concentrations of the model complexes that inhibited the bacterial growth after specified time and temperature.

Effect of Complexes 1−3 on the Bacterial Growth by Crystal Violet Staining. Antibacterial activities of **1**−**3** on *Staphylococcus aureus*, SA96 were visually examined by microscopic assay. Briefly, 10^7 CFU/mL bacterial cells taken from 18 h grown culture, were inoculated with MICs and 1/2 MICs of each of the cobalt(II) complexes in freshly prepared LB medium into 35 mm Petri dishes containing sterile glass cover slips. The control sets were prepared with 1% DMSO (v/v) and same amount of bacterial inoculum in the media in the absence of any cobalt(II) complex. They were incubated at 37 °C for 24 h. Then, the spent media were carefully discarded, and the samples were washed properly with sterile 1× PBS to remove the unbound cells. Subsequently, the samples were fixed with absolute methanol for 15 min and dried at room temperature. Then, a solution of crystal violet (2%) was used to stain the samples for 2 min and washed the excess stain with 1× PBS. Thereafter, 0.33% iodine solution was used for 1 min which serves as a mordant. The samples were rinsed with absolute ethanol until the violet color disappeared, followed by mounting the cover slips with glycerol on the cleaned glass slides. The slides were then observed under a light microscope with 40× magnification.

Effect of Complexes 1−3 on the Bacterial Cell Membrane by Assessing the Cellular Leakage. The mechanistic aspect of antibacterial activities of complexes **1**−**3** against *Staphylococcus aureus*, SA96 was studied by measuring the released cellular components, such as DNA. The underlying principle behind carrying out this particular experiment is that, if the bacterial cell membrane is

damaged by the model complexes, the release of DNA takes place from the bacterial cells through the membrane leakage. Consequently, we can measure the absorbance at 260 nm to determine the amount of DNA released from the cells. This experiment was performed following the previously reported method with slight modification.[100] Briefly, 10^7 CFU/mL bacterial cells were inoculated with fresh LB media containing MICs and 1/2 MICs of **1**−**3** and incubated at 37 °C under stirring conditions. Control sets were also prepared using the same proportion of bacterial inoculum and 1% (v/v) DMSO. Then, in every 1 h interval, 1 mL of sample solution from each set was taken out for 5 h, followed by centrifugation (REMI, CPR-30 PLUS) at 10,000 rpm at 4 °C. After that, the absorbance values of the supernatants were measured at 260 nm employing a Shimadzu UV 1800 spectrophotometer to determine the amount of DNA that was released from each sample at different times.

Study of Combinatorial Effect of Complexes 1−3 with Gentamicin against *Staphylococcus aureus*, SA96. The combinatorial activity of complexes **1**−**3** with commercially available antibiotic, gentamicin was assessed against *Staphylococcus aureus*, SA96. In order to perform this experiment, the MIC of gentamicin against this bacterial strain was determined, and 1/2 and 1/4 of MICs were calculated. Then, 5×10^5 CFU/mL cells were seeded into 200 μL MH broth in sterile 96-well microtiter plate consisting of 1/2 and 1/4 MICs of **1**−**3** and gentamicin individually, as well as in the combination strategy. Control sets were prepared with the same proportion of bacterial inoculum containing only 1% (v/v) DMSO instead of any model cobalt complex. Thereafter, the plate was incubated overnight at 37 °C, followed by measurement of absorbance values at 595 nm in a microplate absorbance reader (iMark Microplate Absorbance Reader, Bio-Rad Laboratories).

Statistical Analysis. All the experiments were run in triplicates, including the respective control sets. The presentation of all data was made as the mean ± standard deviation (SD). Analysis of statistical significance between control sets and complex-treated sets was done by performing one way analysis of variance (ANOVA), followed by Dunnett test by utilizing GraphPad Prism software (version 9.0; GraphPad Software, Inc., USA). *P*-values <0.05 were regarded as statistically significant.

AUTHOR INFORMATION

Corresponding Author

Manindranath Bera − *Department of Chemistry, University of Kalyani, Kalyani, West Bengal 741235, India;* orcid.org/0000-0001-6230-5756; Phone: +91-33-25828282x306; Email: mbera2009@klyuniv.ac.in; Fax: +91-33-25828282

Authors

Sujan Sk − *Department of Chemistry, University of Kalyani, Kalyani, West Bengal 741235, India*

Samik Biswas − *Department of Microbiology, University of Kalyani, Kalyani, West Bengal 741235, India*

Nityananda Dutta − *Department of Chemistry, University of Kalyani, Kalyani, West Bengal 741235, India*

Arpan Das − *Department of Chemical Sciences, Indian Institute of Science Education & Research-Kolkata, Mohanpur, West Bengal 741246, India*

Nithin Suryadevara − *Institute of Quantum Materials and Technologies, Karlsruhe Institute of Technology (KIT), 76344 Eggenstein-Leopoldshafen, Germany*

Gonela Vijaykumar − *Catalysis and Fine Chemicals Department, CSIR-Indian Institute of Chemical Technology, Hyderabad 500607, India;* orcid.org/0000-0002-1249-7347

Pradip Bhunia − *Department of Chemistry, University College of Science, University of Calcutta, Kolkata 700009, India*

Mario Ruben − *Institute of Quantum Materials and Technologies and Institute of Nanotechnology, Karlsruhe Institute of Technology (KIT), 76344 Eggenstein-Leopoldshafen, Germany; Institut de Science et d'Ingénierie Supramolaiculaires-ISIS, Strasbourg CedexF-67083, France*

Supratim Mandal − *Department of Microbiology, University of Kalyani, Kalyani, West Bengal 741235, India*

Notes

The authors declare no competing financial interest.

ACKNOWLEDGMENTS

The authors sincerely acknowledge the Department of Science, Technology and Biotechnology, West Bengal, India for the funding and financial support (Grant No.: ST/P/S&T/15G-18/2019). The DST-FIST (Level-2; SR/FST/CS-II/2019/96) program in the Department of Chemistry, University of Kalyani is greatly acknowledged for offering the instrumental support. N.D. is thankful to CSIR, New Delhi for supporting individual Senior Research Fellowship. S.S. is thankful to UGC, New Delhi for offering Junior Research Fellowship.

REFERENCES

(1) (a) Xiao, D. J.; Gonzalez, M. I.; Darago, L. E.; Vogiatzis, K. D.; Haldoupis, E.; Gagliardi, L.; Long, J. R. Selective, Tunable O_2 Binding in Cobalt(II)-Triazolate/Pyrazolate Metal-Organic Frameworks. *J. Am. Chem. Soc.* **2016**, *138*, 7161−7170. (b) Liu, Z.; He, W.; Guo, Z. Metal Coordination in Photoluminescent Sensing. *Chem. Soc. Rev.* **2013**, *42*, 1568−1600. (c) Jana, A.; Kundu, P.; Paul, S.; Kondaiah, P.; Chakravarty, A. R. Cobalt(III) Complexes for Light-Activated Delivery of Acetylacetonate-BODIPY, Cellular Imaging, and Photodynamic Therapy. *Inorg. Chem.* **2022**, *61*, 6837−6851. (d) Paul, A.; Gupta, A.; Konar, S. Magnetic Transition in Organic Radicals: The Crystal Engineering Aspects. *Cryst. Growth Des.* **2021**, *21*, 5473−5489. (e) Ma, X. F.; Wang, Z.; Chen, X. L.; Kurmoo, M.; Zeng, M. H. Ligand Effect on the Single-Molecule Magnetism of Tetranuclear Co(II) Cubane. *Inorg. Chem.* **2017**, *56*, 15178−15186.

(2) (a) Plyuta, N.; Petrusenko, S.; Kokozay, V. N.; Cauchy, T.; Lloret, F.; Julve, M.; Cano, J.; Avarvari, N. Field-Induced Mononuclear Cobalt(II) Single-Molecule Magnet (SMM) Based on a Benzothiadiazole-Ortho-Vanillin Ligand. *Dalton Trans.* **2022**, *51*, 4760−4771. (b) Pandit, N. R.; Bej, S.; Mondal, A.; Ghosh, M.; Kostakis, G. E.; Powell, A. K.; Banerjee, P.; Biswas, B. Exploratory

Studies on Azido-Bridged Complexes (Ni^{2+} & Mn^{2+}) as Dual Colourimetric Chemosensors for S^{2-} and Ag^{+}: Combined Experimtal and Theoretical Outcome with Real Field Application. *Dalton Trans.* **2020**, *49*, 13090–13099. (c) Verani, C. N.; Rentschler, E.; Weyhermüller, T.; Bill, E.; Chaudhuri, P. Exchange Coupling in a Bis(heterodinuclear) $[Cu^{II}Ni^{II}]_2$ and a Linear Heterotrinuclear Complex $Co^{III}Cu^{II}Ni^{II}$: Synthesis, Structures and Properties. *J. Chem. Soc., Dalton Trans.* **2000**, 251–258. (d) Pandit, N. R.; Bej, S.; Banerjee, P.; Biswas, B. Unveiling Role of Metals in Mononuclear Metal-Complexes for Chemodosimetric Detection of S^{2-} from Aqueous Medium: Experimental and DFT Corroboration with Real-Field Application. *ChemistrySelect* **2022**, *7*, No. e202200307.

(3) Kobayashi, F.; Ohtani, R.; Nakamura, M.; Lindoy, L. F.; Hayami, S. Slow Magnetic Relaxation Triggered by a Structural Phase Transition in Long-Chain-Alkylated Cobalt(II) Single-Ion Magnets. *Inorg. Chem.* **2019**, *58*, 7409–7415.

(4) Hossain, S. M.; Kamilya, S.; Ghosh, S.; Herchel, R.; Kiskin, M. A.; Mehta, S.; Mondal, A. Tuning of Dimensionality and Nuclearity as a Function of Ligand Field Modulation Resulting in Field-Induced Cobalt(II) Single-Ion Magnet. *Cryst. Growth Des.* **2023**, *23*, 1656–1667.

(5) Tangoulis, V.; Lalia-Kantouri, M.; Gdaniec, M.; Papadopoulos, C.; Miletic, V.; Czapik, A. New Type of Single Chain Magnet: Pseudo-One-Dimensional Chain of High-Spin Co(II) Exhibiting Ferromagnetic Intrachain Interactions. *Inorg. Chem.* **2013**, *52*, 6559–6569.

(6) Mondal, A.; Kharwar, A. K.; Konar, S. Sizeable Effect of Lattice Solvent on Field Induced Slow Magnetic Relaxation in Seven Coordinated Co^{II} Complexes. *Inorg. Chem.* **2019**, *58*, 10686–10693.

(7) Sanda, S.; Parshamoni, S.; Adhikary, A.; Konar, S. A Family of Metal-Organic Frameworks Based on Carboxylates and a Neutral, Long, and Rigid Ligand: Their Structural Revelation, Magnetic, and Luminescent Property Study. *Cryst. Growth Des.* **2013**, *13*, 5442–5449.

(8) Langley, S.; Heliwell, M.; Sessoli, R.; Teat, S. J.; Winpenny, R. P. E. Synthesis and Structural and Magnetic Characterization of Cobalt(II) Phosphonate Cage Compounds. *Inorg. Chem.* **2008**, *47*, 497–507.

(9) Ferguson, A.; Parkin, A.; Sanchez-Benítez, J.; Kamenev, J.; Wernsdorfer, W.; Murrie, M. A Mixed-Valence Co_7 Single-Molecule Magnet with C_3 Symmetry. *Chem. Commun.* **2007**, 3473–3475.

(10) Miyasaka, H.; Julve, M.; Yamashita, M.; Clerac, R. Slow Dynamics of the Magnetization in One-Dimensional Coordination Polymers: Single-Chain Magnets. *Inorg. Chem.* **2009**, *48*, 3420–3437.

(11) Pardo, E.; García-Ruiz, R.; Lloret, F.; Faus, J.; Julve, M.; Journaux, Y.; Novak, M. A.; Delgado, F. S.; Ruiz-Perez, C. Ligand Design for Heterobimetallic Single-Chain Magnets: Synthesis, Crystal Structures, and Magnetic Properties of $M^{II}Cu^{II}$ (M=Mn, Co) Chains with Sterically Hindered Methyl-Substituted Phenyloxamate Bridging Ligands. *Chem. – Eur. J.* **2007**, *13*, 2054–2066.

(12) Cahier, B.; Maurice, R.; Bolvin, H.; Mallah, T.; Guihery, N. Tools for Predicting the Nature and Magnitude of Magnetic Anisotropy in Transition Metal Complexes: Application to Co(II) Complexes. *Magnetochemistry* **2016**, *2*, 31.

(13) Piwowarska, D.; Gnutek, P.; Rudowicz, C. Origin of the Ground Kramers Doublets for $Co^{2+}(3d^7)$ Ions with the Effective Spin $^3/_2$ Versus the Fictitious 'Spin' $^1/_2$. *Appl. Magn. Reson.* **2019**, *50*, 797–808.

(14) Gómez-Coca, S.; Cremades, E.; Aliaga-Alcalde, N.; Ruíz, E. Mononuclear Single-Molecule Magnets: Tailoring the Magnetic Anisotropy of First-Row Transition-Metal Complexes. *J. Am. Chem. Soc.* **2013**, *135*, 7010–7018.

(15) Zadrozny, J. M.; Long, J. R. Slow Magnetic Relaxation at Zero Field in the Tetrahedral Complex $[Co(SPh)_4]_2^-$. *J. Am. Chem. Soc.* **2011**, *133*, 20732–20734.

(16) Saber, M. R.; Dunbar, K. R. Ligands Effects on the Magnetic Anisotropy of Tetrahedral Cobalt Complexes. *Chem. Commun.* **2014**, *50*, 12266–12269.

(17) Feng, M.; Tong, M. L. Single Ion Magnets from 3d to 5f: Developments and Strategies. *Chem. – Eur. J.* **2018**, *24*, 7574–7594.

(18) Bar, A. K.; Pichon, C.; Sutter, J. P. Magnetic Anisotropy in Two to Eight-Coordinated Transition-Metal Complexes: Recent Developments in Molecular Magnetism. *Coord. Chem. Rev.* **2016**, *308*, 346–380.

(19) Liu, J. J.; Jiang, S. D.; Neugebauer, P.; van Slageren, J.; Lan, Y.; Wernsdorfer, W.; Wang, B. W.; Gao, S. Magnetic and HFEPR Studies of Exchange Coupling in a Series of μ-Cl Dicobalt Complexes. *Inorg. Chem.* **2017**, *56*, 2417–2425.

(20) Schweinfurth, D.; Rechkemmer, Y.; Hohloch, S.; Deibel, N.; Peremykin, I.; Fiedler, J.; Marx, R.; Neugebauer, P.; van Slageren, J.; Sarkar, B. Redox-Induced Spin-State Switching and Mixed Valency in Quinonoid-Bridged Dicobalt Complexes. *Chem. – Eur. J.* **2014**, *20*, 3475–3486.

(21) DeLucia, A. A.; Kelly, K. A.; Herrera, K. A.; Gray, D. L.; Olshansky, L. Intramolecular Hydrogen-Bond Interactions Tune Reactivity in Biomimetic Bis(μ-hydroxo)dicobalt Complexes. *Inorg. Chem.* **2021**, *60*, 15599–15609.

(22) (a) Bera, M.; Curtiss, A. B. S.; Musie, G. T.; Powell, D. R. New Dinuclear Cobalt(II) and Zinc(II) Complexes of a Carboxylate-Rich Dinucleating Ligand: Synthesis, Structure, Spectroscopic Characterization, and Their Interactions with Sugars. *Inorg. Chem.* **2012**, *51*, 12093–12101. (b) Majumder, A.; Dutta, N.; Haldar, S.; Das, A.; Carrella, L.; Bera, M. Aromatic Dicarboxylate Incorporated New Di- and Tetranuclear Cobalt(II) Complexes: Synthetic and Structural Aspects, and Evaluation of Properties and Catalytic Activity. *Inorg. Chim. Acta* **2020**, *510*, No. 119752. (c) Bera, M.; Patra, A. Study of Potential Binding of Biologically Important Sugars with a Dinuclear Cobalt(II) Complex. *Carbohydr. Res.* **2011**, *346*, 733–738.

(23) Jie, S.; Ai, P.; Li, B. G. Highly Active and Stereospecific Polymerization of 1,3-butadiene Catalyzed by Dinuclear Cobalt(II) Complexes Bearing 3-aryliminomethyl-2-hydroxybenzaldehydes. *Dalton Trans.* **2011**, *40*, 10975–10982.

(24) Mondal, S.; Bera, S.; Maity, S.; Ghosh, P. Cobalt Ion Promoted Redox Cascade: A Route to Spiro Oxazine-Oxazepine Derivatives and a Dinuclear Cobalt Complex of an N-(1,4-Naphthoquinone)-oaminophenol Derivative. *Inorg. Chem.* **2017**, *56*, 13194–13204.

(25) Daumann, L. J.; Schenk, G.; Ollis, D. L.; Gahan, L. R. Spectroscopic and Mechanistic Studies of Dinuclear Metallohydrolases and Their Biomimetic Complexes. *Dalton Trans.* **2014**, *43*, 910–928.

(26) Wang, J. P.; Liu, W. T.; Yu, M.; Ji, X. Y.; Liu, J. L.; Chi, M. Z.; Starikova, A. A.; Tao, J. One-Step versus Two-Step Valence Tautomeric Transitions in Tetraoxolene-Bridged Dinuclear Cobalt Compounds. *Inorg. Chem.* **2022**, *61*, 4428–4441.

(27) Ishizaka, Y.; Nakajima, Y. Synthesis and Characterization of Silyl-Bridged Dinuclear Cobalt Complexes Supported by an N-Heterocyclic Carbene. *Organometallics* **2019**, *38*, 888–893.

(28) Ghosh, S.; Kamilya, S.; Rouzières, M.; Herchel, R.; Mehta, S.; Mondal, A. Reversible Spin-State Switching and Tuning of Nuclearity and Dimensionality *via* Nonlinear Pseudohalides in Cobalt(II) Complexes. *Inorg. Chem.* **2020**, *59*, 17638–17649.

(29) Fondo, M.; Doejo, J.; García-Deibe, A. M.; Sanmartín-Matalobos, J.; Vicente, R.; El-Fallah, M. S.; Amoza, M.; Ruiz, E. Predetermined Ferromagnetic Coupling via Strict Control of M-O-M Angles. *Inorg. Chem.* **2016**, *55*, 11707–11715.

(30) Alam, R.; Kaberi, P.; Bikash, K. S.; Malay, D.; Nabanita, P.; Shyamal, K. S.; Mahammad, A. Synthesis, Structure, Catalytic and Magnetic Properties of a Pyrazole Based Five Coordinated Dinuclear Cobalt(II) Complex. *Polyhedron* **2016**, *106*, 84–91.

(31) Long, T.; Yang, J.; Moorthy, S.; Shao, D.; Singh, S. K.; Zhang, Y. Z. Incorporating Highly Anisotropic Four-Coordinate Co(II) Ions within One-Dimensional Coordination Chains. *Cryst. Growth Des.* **2023**, *23*, 2980–2987.

(32) Fabelo, O.; Canadillas-Delgado, L.; Pasán, J.; Delgado, F. S.; Lloret, F.; Cano, J.; Julve, M.; Ruiz-Pérez, C. Study of the Influence of the Bridge on the Magnetic Coupling in Cobalt(II) Complexes. *Inorg. Chem.* **2009**, *48*, 11342–11351.

(33) Casanova, I.; Duran, M. L.; Viqueira, J.; Sousa-Pedrares, A.; Zani, F.; Real, J. A.; García-Vázquez, J. A. Metal Complexes of a Novel Heterocyclic Benzimidazole Ligand Formed by Rearrangement Cyclization of the Corresponding Schiff Base: Electrosynthesis, Structural Characterization and Antimicrobial Activity. *Dalton Trans.* **2018**, *47*, 4325−4340.
(34) Reger, D. L.; Pascui, A. E.; Foley, E. A.; Smith, M. D.; Jezierska, J.; Ozarowski, A. Dinuclear Metallacycles with Single M-O(H)-M Bridges [M = Fe(II), Co(II), Ni(II), Cu(II)]: Effects of Large Bridging Angles on Structure and Antiferromagnetic Superexchange Interactions. *Inorg. Chem.* **2014**, *53*, 1975−1988.
(35) (a) Kharwar, A. K.; Mondal, A.; Sarkar, A.; Rajaraman, G.; Konar, S. Modulation of Magnetic Anisotropy and Exchange Interaction in Phenoxide-Bridged Dinuclear Co(II) Complexes. *Inorg. Chem.* **2021**, *60*, 11948−11956. (b) Ali, S. I.; Kremer, R. K.; Johnson, M. Hydrothermal Synthesis and Magnetic Characterization of the Quaternary Oxide $CoMo_2Sb_2O_{10}$. *Inorg. Chem.* **2016**, *55*, 11490−11496.
(36) Silva, R. M.; Smith, M. D.; Gardinier, J. R. Anion- and Solvent-Directed Assembly in Silver Bis(thioimidazolyl)methane Chemistry and the Silver-Sulfur Interaction. *Inorg. Chem.* **2006**, *45*, 2132−2142.
(37) (a) Gale, P. A.; Quesada, R. Anion Coordination and Anion-Templated Assembly: Highlights from 2002 to 2004. *Coord. Chem. Rev.* **2006**, *250*, 3219−3244. (b) Gale, P. A. Anion Coordination and Anion-Directed Assembly: Highlights from 1997 and 1998. *Coord. Chem. Rev.* **2000**, *199*, 181−233.
(38) Forster, P. M.; Stock, N.; Cheetham, A. K. A High-Throughput Investigation of the Role of pH, Temperature, Concentration, and Time on the Synthesis of Hybrid Inorganic-Organic Materials. *Angew. Chem., Int. Ed.* **2005**, *44*, 7608−7611.
(39) Kumar, R. S.; Arunachalam, S. Synthesis, Micellar Properties, DNA Binding and Antimicrobial Studies of Some Surfactant-Cobalt(III) Complexes. *Biophys. Chem.* **2008**, *136*, 136−144.
(40) Nagababu, P.; Latha, J. N. L.; Pallavi, P.; Harish, S.; Satyanarayana, S. Studies on Antimicrobial Activity of Cobalt(III) Ethylenediamine Complexes. *Can. J. Microbiol.* **2006**, *52*, 1247−1254.
(41) Ohui, K.; Afanasenko, E.; Bacher, F.; Ting, R. L. X.; Zafar, A.; Blanco-Cabra, N.; Torrents, E.; Domotor, O.; May, N. V.; Darvasiova, D.; Enyedy, E. A.; Popović-Bijelić, A.; Reynisson, J.; Rapta, P.; Babak, M. V.; Pastorin, G.; Arion, V. B. New Water-Soluble Copper(II) Complexes with Morpholine-Thiosemicarbazone Hybrids: Insights into the Anticancer and Antibacterial Mode of Action. *J. Med. Chem.* **2019**, *62*, 512−530.
(42) Kargar, H.; Ardakani, A. A.; Tahir, M. N.; Ashfaq, M.; Munawar, K. S. Synthesis, Spectral Characterization, Crystal Structure and Antibacterial Activity of Nickel(II), Copper(II) and Zinc(II) Complexes Containing ONNO Donor Schiff Base Ligands. *J. Mol. Struct.* **2021**, *1233*, No. 130112.
(43) (a) Wang, X.; He, S.; Yuan, L.; Deng, H.; Zhang, Z. Synthesis, Structure Characterization, and Antioxidant and Antibacterial Activity Study of Iso-orientin-Zinc Complex. *J. Agric. Food Chem.* **2021**, *69*, 3952−3964. (b) Passieux, R.; Sudre, G.; Montembault, A.; Renard, M.; Hagege, A.; Alcouffe, P.; Haddane, A.; Vandesteene, M.; Boucard, N.; Bordenave, L.; David, L. Cytocompatibility/Antibacterial Activity Trade-off for Knittable Wet-Spun Chitosan Monofilaments Functionalized by the In Situ Incorporation of Cu^{2+} and Zn^{2+}. *ACS Biomater. Sci. Eng.* **2022**, *8*, 1735−1748. (c) Nicolafrancesco, C.; Porcaro, F.; Pis, I.; Nappini, S.; Simonelli, L.; Marini, C.; Frangipani, E.; Visaggio, D.; Visca, P.; Mobilio, S.; Meneghini, C.; Fratoddi, I.; Iucci, G.; Battocchio, C. Gallium- and Iron-Pyoverdine Coordination Compounds Investigated by X-ray Photoelectron Spectroscopy and X-ray Absorption Spectroscopy. *Inorg. Chem.* **2019**, *58*, 4935−4944. (d) Best, M. G.; Cunha-Reis, C.; Ganin, A. Y.; Sousa, A.; Johnston, J.; Oliveira, A. L.; Smith, D. G. E.; Yiu, H. H. P.; Cooper, I. R. Antimicrobial Properties of Gallium(III) and Iron(III)-Loaded Polysaccharides Affecting the Growth of *Escherichia coli*, *Staphylococcus aureus,* and *Pseudomonas aeruginosa*, In Vitro. *ACS Appl. Bio Mater.* **2020**, *3*, 7589−7597.
(44) (a) Banerjee, S.; Chakravarty, A. R. Metal Complexes of Curcumin for Cellular Imaging, Targeting, and Photoinduced Anticancer Activity. *Acc. Chem. Res.* **2015**, *48*, 2075−2083. (b) Portelinha, J.; Duay, S. S.; Yu, S. I.; Heilemann, K.; Libardo, M. D. J.; Juliano, S. A.; Klassen, J. L.; Angeles-Boza, A. M. Antimicrobial Peptides and Copper(II) Ions: Novel Therapeutic Opportunities. *Chem. Rev.* **2021**, *121*, 2648−2712. (c) Zhang, W.; Shi, T.; Ding, G.; Punyapitak, D.; Zhu, J.; Guo, D.; Zhang, Z.; Li, J.; Cao, Y. Nanosilica Schiff-Base Copper(II) Complexes with Sustainable Antimicrobial Activity against Bacteria and Reduced Risk of Harm to Plant and Environment. *ACS Sustainable Chem. Eng.* **2017**, *5*, 502−509.
(45) Jiang, X.; Zhou, T.; Bai, R.; Xie, Y. Hydroxypyridinone-Based Iron Chelators with Broad-Ranging Biological Activities. *J. Med. Chem.* **2020**, *63*, 14470−14501.
(46) Ajibola, A. A.; Obaleye, J. A.; Sieron, L.; Maniukiewicz, W.; Wojciechowska, A.; Ozarowski, A. Structural, Spectroscopic Insights, and Antimicrobial Properties of Mononuclear and Dinuclear Metal-(II) Carboxylate Derivatives with Metronidazole. *Polyhedron* **2021**, *194*, No. 114931.
(47) Saleem, A.; Kobielska, P. A.; Harms, K.; Katsikogianni, M. G.; Telford, R.; Novitchi, G.; Nayak, S. Transition Metal Complexes of a Versatile Polyalkoxy Oxazolidine-Based Ligand Derived from *In Situ* Cyclization. *Dalton Trans.* **2018**, *47*, 6156−6165.
(48) Huy, T. X. N.; Nguyen, T. T.; Reyes, A. W. B.; Kim, H.; Min, W.; Lee, H. H.; Lee, J. H.; Kim, S. Cobalt (II) Chloride Regulates the Invasion and Survival of *Brucella abortus* 544 in RAW 264.7 Cells and B6 Mice. *Pathogens* **2022**, *11*, 596.
(49) (a) Abass, A. A.; Abdulridha, W. M.; Alaarage, W. K.; Abdulrudha, N. H.; Haider, J. Evaluating the Antibacterial Effect of Cobalt Nanoparticles Against Multi-Drug Resistant Pathogens. *J. Med. Life* **2021**, *14*, 823−833. (b) Suvarta, K. D.; Gurunath, N. H.; Gavade Shubhangi, M. J.; Sachinkumar, P. R.; Kishor, G. V. Biogenic Synthesis of Cobalt Nanoparticles Using Hibiscus Cannabinus Leaf Extract and Their Antibacterial Activity. *Res. J. Chem. Environ.* **2020**, *24*, 9−13. (c) Shahzadi, T.; Zaib, M.; Riaz, T.; Shehzadi, S.; Abbasi, M. A.; Shahid, M. Synthesis of Eco-friendly Cobalt Nanoparticles Using Celosia Argentea Plant Extract and Their Efficacy Studies as Antioxidant, Antibacterial, Hemolytic and Catalytical Agent. *Arab. J. Sci. Eng.* **2019**, *44*, 6435−6444.
(50) Nirbhavane, H. M.; Bagde, U. S. Study on Mechanism of Cobalt Resistance in Enterobacter Species. *Indian J. Microbiol. Res.* **2019**, *6*, 22−29.
(51) (a) Mukherjee, S.; Abboud, K. A.; Wernsdorfer, W.; Christou, G. Comproportionation Reactions to Manganese(III/IV) Pivalate Clusters: A New Half-Integer Spin Single-Molecule Magnet. *Inorg. Chem.* **2013**, *52*, 873−884. (b) Li, J.; Li, B.; Pan, M.; Liu, B.; Cheng, J.; Li, R.; Gao, X.; Wang, S.; Hou, H.; Liu, Z. Five Multidimensional Co(II)-Complexes (Zero-Dimensional to Three-Dimensional) Derived from an Asymmetric 5-(Pyridin-3-yl)-1*H*-pyrazole-3-carboxylic Acid: Syntheses, Structures, and Magnetic Properties. *Cryst. Growth Des.* **2017**, *17*, 2975−2986.
(52) (a) Sk, S.; Majumder, A.; Sow, P.; Samadder, A.; Bera, M. Exploring a New Family of Designer Copper(II) Complexes of Anthracene-Appended Polyfunctional Organic Assembly Displaying Potential Anticancer Activity *via* Cytochrome *c* Mediated Mitochondrial Apoptotic Pathway. *J. Inorg. Biochem.* **2023**, *243*, No. 112182. (b) Majumder, A.; Sarkar, C.; Das, I.; Sk, S.; Bandyopadhyay, S.; Mandal, S.; Bera, M. Design, Synthesis and Evaluation of a Series of Zinc(II) Complexes of Anthracene-Affixed Multifunctional Organic Assembly as Potential Antibacterial and Antibiofilm Agents against Methicillin-Resistant *Staphylococcus aureus*. *ACS Appl. Mater. Interfaces* **2023**, *15*, 22781−22804.
(53) Jia, H. P.; Li, W.; Ju, Z. F.; Zhang, J. Synthesis, Structure and Magnetism of Metal-Organic Framework Materials with Doubly Pillared Layers. *Eur. J. Inorg. Chem.* **2006**, *2006*, 4264.
(54) Rueff, J. M.; Masciocchi, N.; Rabu, P.; Sironi, A.; Skoulios, A. Structure and Magnetism of a Polycrystalline Transition Metal Soap-$Co^{II}[OOC(CH_2)_{10}COO](H_2O)_2$. *Eur. J. Inorg. Chem.* **2001**, *2001*, 2843−2848.

(55) Mishra, V.; Lloret, F.; Mukherjee, R. Coordination Versatility of 1,3-bis[3-(2-pyridyl)pyrazol-1-yl]propane: Co(II) and Ni(II) Complexes. *Inorg. Chim. Acta* **2006**, *359*, 4053−4062.
(56) (a) Kitaura, R.; Kitagawa, S.; Kubota, Y.; Kobayashi, T. C.; Kindo, K.; Mita, Y.; Matsuo, A.; Kobayashi, M.; Chang, H. C.; Ozawa, T. C.; Suzuki, M.; Sakata, M.; Takata, M. Formation of a One-Dimensional Array of Oxygen in a Microporous Metal-Organic Solid. *Science* **2002**, *298*, 2358−2361. (b) Pavlishchuk, V. V.; Koval, I. A.; Goreshnik, E.; Addison, A. W.; van Albada, G. A.; Reedijk, J. The First Example of a True "Turnbull's Blue" Family Compound with Trapped Iron Oxidation States. *Eur. J. Inorg. Chem.* **2001**, *2001*, 297−301. (c) Swiegers, G. F.; Malefetse, T. J. New Self-Assembled Structural Motifs in Coordination Chemistry. *Chem. Rev.* **2000**, *100*, 3483−3538.
(57) Majumder, A.; Dutta, N.; Dey, S.; Sow, P.; Samadder, A.; Vijaykumar, G.; Rangan, K.; Bera, M. A Family of $[Zn_6]$ Complexes from the Carboxylate-Bridge-Supported Assembly of $[Zn_2]$ Building Units: Synthetic, Structural, Spectroscopic, and Systematic Biological Studies. *Inorg. Chem.* **2021**, *60*, 17608−17626.
(58) Patra, A.; Haldar, S.; Vijaykumar, G.; Carrella, L.; Ghosh, A. K.; Bera, M. New Symmetrical Dinucleating Ligand Based Assembly of Bridged Dicopper(II) and Dizinc(II) Centers: Synthesis, Structure, Spectroscopy, Magnetic Properties and Glycoside Hydrolysis. *Inorg. Chim. Acta* **2015**, *436*, 195−204.
(59) Dutta, N.; Haldar, S.; Vijaykumar, G.; Paul, S.; Chattopadhyay, A. P.; Carrella, L.; Bera, M. Phosphatase-like Activity of Tetranuclear Iron(III) and Zinc(II) Complexes. *Inorg. Chem.* **2018**, *57*, 10802−10820.
(60) Giri, G. C.; Patra, A.; Vijaykumar, G.; Carrella, L.; Bera, M. Hydrolytically Active Tetranuclear $[Ni^{II}_2]_2$ Complexes: Synthesis, Structure. Spectroscopy and Phosphoester Hydrolysis. *RSC Adv.* **2015**, *5*, 99270−99283.
(61) Haldar, S.; Vijaykumar, G.; Carrella, L.; Batha, S.; Musie, G. T.; Bera, M. Inorganic Phosphate and Arsenate within New Tetranuclear Copper and Zinc Complexes: Syntheses, Crystal Structures, Magnetic, Electrochemical, and Thermal Studies. *ACS Omega* **2017**, *2*, 1535−1549.
(62) Haldar, S.; Dutta, N.; Vijaykumar, G.; Das, A.; Carrella, L.; Oliver, A.; Bera, M. Synthesis, Structure and Properties of New Heterometallic Octanuclear $Li_2Na_2Cu_4$ and Decanuclear Li_2Zn_8 Complexes. *Polyhedron* **2019**, *172*, 58−66.
(63) Sarkar, C.; Sk, S.; Majumder, A.; Haldar, S.; Vijaykumar, G.; Bera, M. Synthesis, Structure, Thermal and Magnetic Properties of New Tetranuclear Copper(II) Complex Supported by Multidentate Ligand and Glutarate Functionality. *J. Mol. Struct.* **2023**, *1277*, No. 134855.
(64) Majumder, A.; Sk, S.; Das, A.; Vijaykumar, G.; Sahoo, M. K.; Behera, J. N.; Bera, M. Ancillary-Ligand-Assisted Variation in Nuclearities Leading to the Formation of Di-, Tri-, and Tetranuclear Copper(II) Complexes with Multifaceted Carboxylate Coordination Chemistry. *ACS Omega* **2022**, *7*, 39985−39997.
(65) Haldar, S.; Vijaykumar, G.; Carrella, L.; Musie, G. T.; Bera, M. Structure and Properties of A Novel Staircase-Like Decanuclear $[Cu^{II}_{10}]$ Cluster Supported by Carbonate and Carboxylate Bridges. *New J. Chem.* **2018**, *42*, 1276−1283.
(66) Geary, W. J. The Use of Conductivity Measurements in Organic Solvents for the Characterisation of Coordination Compounds. *Coord. Chem. Rev.* **1971**, *7*, 81−122.
(67) Abumelha, H. M.; Alkhatib, F.; Alzahrani, S.; Abualnaja, M.; Alsaigh, S.; Alfaifi, M. Y.; Althagafi, I.; El-Metwaly, N. Synthesis and Characterization for Pharmaceutical Models from Co(II), Ni(II) and Cu(II)-Thiophene Complexes: Apoptosis, Various Theoretical Studies and Pharmacophore Modeling. *J. Mol. Liq.* **2021**, *328*, No. 115483.
(68) Wang, J.; Cui, C.; Gao, G.; Zhou, X.; Wu, J.; Yang, H.; Li, Q.; Wu, G. A New Method to Prepare Vanadium Oxide Nano-Urchins as a Cathode for Lithium Ion Batteries. *RSC Adv.* **2015**, *5*, 47522−47528.
(69) Ekennia, A. C.; Onwudiwe, D. C.; Olasunkanmi, L. O.; Osowole, A. A.; Ebenso, E. E. Synthesis, DFT Calculation, and Antimicrobial Studies of Novel Zn(II), Co(II), Cu(II), and Mn(II) Heteroleptic Complexes Containing Benzoylacetone and Dithiocarbamate. *Bioinorg. Chem. Appl.* **2015**, *2015*, No. 789063.
(70) Deacon, G. B.; Phillips, R. J. Relationships Between the Carbon Oxygen Stretching Frequencies of Carboxylato Complexes and the Type of Carboxylate Coordination. *Coord. Chem. Rev.* **1980**, *33*, 227−250.
(71) Zelenák, V.; Vargová, Z.; Gyoryová, K. Correlation of Infrared Spectra of Zinc(II) Carboxylates with Their Structures. *Spectrochim. Acta A Mol. Biomol. Spectrosc.* **2007**, *66*, 262−272.
(72) Arora, H.; Lloret, F.; Mukherjee, R. Molecular Squares of Ni^{II} and Cu^{II}: Ferromagnetic Exchange Interaction Mediated by *syn-anti* Carboxylate-Bridging. *Dalton Trans.* **2009**, 9759−9769.
(73) Murray, A. V.; Wacker, J. N.; Bertke, J. A.; Knope, K. E. Synthesis, Characterization, and Solid-State Structural Chemistry of Uranium(IV) Aliphatic Dicarboxylates. *Cryst. Growth Des.* **2021**, *21*, 2429−2444.
(74) Hossain, M. J.; Sakiyama, H. Two Typical Cases of Magnetism for Dinuclear High-Spin Cobalt(II) Complexes in Trigonal-Bipyramidal Fields. *Inorg. Chim. Acta* **2002**, *338*, 255−259.
(75) Massoud, S. S.; Quan, L. L.; Gatterer, K.; Albering, J. H.; Fischer, R. C.; Mautner, F. A. Structural Characterization of Five-Coordinate Copper(II), Nickel(II), and Cobalt(II) Thiocyanato Complexes Derived from Bis(2-(3,5-dimethyl-1-pyrazolyl)ethyl)-amine. *Polyhedron* **2012**, *31*, 601−606.
(76) Bera, M.; Curtiss, A. B. S.; Musie, G. T.; Powell, D. R. A New Self-Assembled μ_6-Sulfato Hexanuclear Cobalt(II) Complex of a Symmetric Dinucleating Ligand: Synthesis and X-ray Structural Analysis. *Inorg. Chem. Commun.* **2008**, *11*, 1033−1036.
(77) Bera, M.; Musie, G. T.; Powell, D. R. Synthesis and Characterization of a Novel Cyclic Tetranuclear Co^{II}_4 Cluster Consisting of a Quadrilateral Core. *Inorg. Chem. Commun.* **2010**, *13*, 1029−1031.
(78) Li, L. L.; Li, P.; Zhang, T.; Dong, W. K. Exploration of DFT and Hirshfeld Analyses and Fluorescence Properties of Three Stable Penta-Coordinated Binuclear Co(II) and Zn(II) Bis (salamo)-Based Complexes. *Polyhedron* **2021**, *205*, No. 115301.
(79) Cotton, F. A.; Wilkinson, G. *Adv. Inorg. Chem.*, 5th Ed.; Wiley: NewYork, 1988.
(80) Bailar, J. C.; Emeleus, H. J.; Nythorm, S. R.; Dickenson, A. F. T. *Compr. Inorg. Chem.*, 1st Ed.; Pergamon: Oxford, 1973.
(81) Addison, A. W.; Rao, T. N.; Reedijk, J.; van Rijn, J.; Verschoor, G. C. Synthesis, Structure, and Spectroscopic Properties of Copper-(II) Compounds Containing Nitrogen-Sulphur Donor Ligands; The Crystal and Molecular Structure of Aqua[1,7- bis(*N*-methylbenzimidazol-2′-yl)-2,6-dithiaheptane] Copper(II) Perchlorate. *J. Chem. Soc., Dalton Trans.* **1984**, 1349−1356.
(82) Massoud, S. S.; Perez, Z. E.; Courson, J. R.; Fischer, R. C.; Mautner, F. A.; Vančo, J.; Čajan, M.; Travníček, Z. Slow Magnetic Relaxation in Penta-Coordinate Cobalt(II) Field-Induced Single-Ion Magnets (SIMs) with Easy-Axis Magnetic Anisotropy. *Dalton Trans.* **2020**, *49*, 11715−11726.
(83) Banerjee, A.; Banerjee, S.; Gómez García, C. J.; Benmansour, S.; Chattopadhyay, S. Magnetic Properties of End-to-End Azide-Bridged Tetranuclear Mixed-Valence Cobalt(III)/Cobalt(II) Complexes with Reduced Schiff Base Blocking Ligands and DFT Study. *ACS Omega* **2019**, *4*, 20634−20643.
(84) Mentre, O.; Laachir, A.; Guesmi, S.; Ketatni, E. M.; Saadi, M.; Ammari, L. E.; Esserti, S.; Faize, M.; Bentiss, F. A New Homobimetallic Cobalt(II) Complex Based on the Tetradentate 3,5-Bis(2-pyridyl)-1H-1,2,4-triazole Ligand: Synthesis, Crystal Structure, Hirshfeld Analysis, Spectroscopic Characterization. Magnetic Properties and Antimicrobial Activities. *Polyhedron* **2020**, *189*, No. 114722.
(85) Banerjee, A.; Banerjee, S.; Gómez-García, C. J.; Benmansour, S.; Chattopadhyay, S. Field-Induced Single Molecule Magnet Behavior of a Dinuclear Cobalt(II) Complex: A Combined

Experimental and Theoretical Study. *Dalton Trans.* **2020**, *49*, 16778−16790.
(86) Siluvai, G. S.; Murthy, N. N. X-ray Structure and Spectroscopic Characterization of Divalent Dinuclear Cobalt Complexes Containing Carboxylate- and Phosphodiester- Auxiliary Bridges. *Inorg. Chim. Acta* **2009**, *362*, 3119−3126.
(87) Daumann, L. J.; Comba, P.; Larrabee, J. A.; Schenk, G.; Stranger, R.; Cavigliasso, G.; Gahan, L. R. Synthesis, Magnetic Properties, and Phosphoesterase Activity of Dinuclear Cobalt(II) Complexes. *Inorg. Chem.* **2013**, *52*, 2029−2043.
(88) Tomkowicz, Z.; Ostrovsky, S.; Foro, S.; Calvo-Perez, V.; Haase, W. Magnetooptical and Structural Investigations of Five Dimeric Cobalt(II) Complexes Mimicking Metalloenzyme Active Sites. *Inorg. Chem.* **2012**, *51*, 6046−6055.
(89) Jana, M.; Majumdar, A. C-S Bond Cleavage, Redox Reactions, and Dioxygen Activation by Nonheme Dicobalt(II) Complexes. *Inorg. Chem.* **2018**, *57*, 617−632.
(90) Chen, T.; Li, M.; Liu, J. $\pi-\pi$ Stacking Interaction: A Nondestructive and Facile Means in Material Engineering for Bioapplications. *Cryst. Growth Des.* **2018**, *18*, 2765−2783.
(91) Hunter, C. A.; Sanders, J. K. M. The Nature of pi-pi Interactions. *J. Am. Chem. Soc.* **1990**, *112*, 5525−5534.
(92) Wei, Y.; Dong, Y.; Sun, W.; Hou, Q.; Shi, Q.; Lan, X. Phase Behavior and Heat Capacity of Alkylboron-Capped Cobalt(II) and Nickel(II) Clathrochelates. *Thermochim. Acta* **2022**, *716*, No. 179304.
(93) Abou-Melha, K. S.; Al-Hazmi, G. A.; Althagafi, I.; Alharbi, A.; Shaaban, F.; El-Metwaly, N. M.; El-Bindary, A. A.; El-Bindary, M. A. Synthesis, Characterization, DFT Calculation, DNA Binding and Antimicrobial Activities of Metal Complexes of Dimedone Arylhydrazone. *J. Mol. Liq.* **2021**, *334*, No. 116498.
(94) (a) Roos, B. O.; Taylor, P. R.; Sigbahn, P. E. M. A Complete Active Space SCF Method (CASSCF) Using a Density Matrix Formulated Super-CI Approach. *Chem. Phys.* **1980**, *48*, 157−173. (b) Angeli, C.; Cimiraglia, R.; Evangelisti, S.; Leininger, T.; Marlieu, J. P. Introduction of *n*-electron Valence States for Multireference Perturbation Theory. *J. Chem. Phys.* **2001**, *114*, 10252−10264. (c) Neese, F. Calculation of the Zero-Field Splitting Tensor on the Basis of Hybrid Density Functional and Hartree-Fock Theory. *J. Chem. Phys.* **2007**, *127*, 164112.
(95) Chilton, N. F.; Anderson, R. P.; Turner, L. D.; Soncini, A.; Murray, K. S. *PHI*: A Powerful New Program for the Analysis of Anisotropic Monomeric and Exchange Coupled Polynuclear d- and f-block Complexes. *J. Comput. Chem.* **2013**, *34*, 1164−1175.
(96) Rajnák, C.; Titiš, J. N.; Fuhr, O.; Ruben, M.; Boča, R. Single-Molecule Magnetism in a Pentacoordinate Cobalt (II) Complex Supported by an Antenna Ligand. *Inorg. Chem.* **2014**, *53*, 8200−8202.
(97) (a) Shin, J. W.; Rowthu, S. R.; Hyun, M. Y.; Song, Y. J.; Kim, C.; Kim, B. G.; Min, K. S. Monomeric, Trimeric, and Tetrameric Transition Metal Complexes (Mn, Fe, Co) Containing *N*,*N*-Bis(2-pyridylmethyl)-2-Aminoethanol/−ate: Preparation, Crystal Structure, Molecular Magnetism and Oxidation Catalysis. *Dalton Trans.* **2011**, *40*, 5762−5773. (b) Pham, A. T.; Abbasi, P.; Monache, G. D.; Mazarakioti, E. C.; Rawson, J. M.; Stamatatos, T. C.; Pilkington, M. Magneto-Structural Studies of Two M-O-M Bridged Homochiral Mixed Valence Co(II)/Co(III) Complexes. *Polyhedron* **2019**, *170*, 34−40.
(98) (a) Samulewski, R. B.; da Rocha, J. C.; Fuganti, O.; Stieler, R.; Lang, E. S.; Vaz, M. G. F.; Nunes, F. S. Structure, Spectroelectrochemistry and Magnetic Properties of a Dicobalt(II)-Tetraiminodiphenolate Complex. *J. Mol. Struct.* **2010**, *984*, 354−358. (b) Thakurta, S.; Butcher, R. J.; Gómez-García, C. J.; Garribba, E.; Mitra, S. Synthesis, Structural Aspects and Magnetic Properties of an Unusual 2D Thiocyanato-Bridged Cobalt(II)-Schiff Base Network. *Inorg. Chim. Acta* **2010**, *363*, 3981−3986. (c) Luo, F.; Luo, M. B. Solvothermal In Situ Synthesis of Schiff Base-Containing Dinuclear Cobalt Compound. *Inorg. Chem. Commun.* **2010**, *13*, 319−321. (d) Lin, S. Y.; Xu, G. F.; Zhao, L.; Tang, J.; Liu, G. X. Structure and Magnetic Properties of a μ-Phenoxido-Bridged Dinuclear Cobalt(II) Complex. *Z. Anorg. Allg. Chem.* **2011**, *637*, 720−723. (e) Herchel, R.; Dvořák, Z.; Travníček, Z.; Mikuriya, M.; Louka, F. R.; Mautner, F. A.; Massoud, S. S. Cobalt (II) and Copper (II) Covalently and Noncovalently Dichlorido-Bridged Complexes of an Unsymmetrical Tripodal Pyrazolyl-Pyridyl Amine Ligand: Structures, Magnetism and Cytotoxicity. *Inorg. Chim. Acta* **2016**, *451*, 102−110. (f) Labisbal, E.; Rodríguez, L.; Souto, O.; Sousa-Pedrares, A.; García-Vázquez, J. A.; Romero, J.; Sousa, A.; Yañez, M.; Orallo, F.; Real, J. A. Electrochemical Synthesis and Structural Characterization of Co(II), Ni(II) and Cu(II) Complexes of *N*,*N*-bis(4,5-dimethyl-2-hydroxybenzyl)-*N*-(2-pyridylmethyl)amine. *Dalton Trans.* **2009**, 8644−8656.
(99) (a) Song, X. J.; Xue, X. M. Study on the Magneto-Structural Correlation of a New Dinuclear Cobalt(II) Complex with Double μ-Phenoxo Bridges. *ACS Omega* **2020**, *5*, 8347−8354. (b) Olguín, J. Unusual Metal Centres/Coordination Spheres in Spin Crossover Compounds. *Coord. Chem. Rev.* **2020**, *407*, No. 213148.
(100) Ananda, A. P.; Manukumar, H. M.; Krishnamurthy, N. B.; Nagendra, B. S.; Savitha, K. R. Assessment of Antibacterial Efficacy of a Biocompatible Nanoparticle PC@AgNPs against *Staphylococcus Aureus*. *Microb. Pathog.* **2019**, *126*, 27−39.
(101) (a) Bieganski, P.; Szczupak, L.; Arruebo, M.; Kowalski, K. Brief Survey on Organometalated Antibacterial Drugs and Metal-Based Materials with Antibacterial Activity. *RSC Chem. Biol.* **2021**, *2*, 368−386. (b) Li, X.; Jiang, F.; Liu, M.; Qu, Y.; Lan, Z.; Dai, X.; Huang, C.; Yue, X.; Zhao, S.; Pan, X.; Zhang, C. Synthesis, Characterization, and Bioactivities of Polysaccharide Metal Complexes: A Review. *J. Agric. Food Chem.* **2022**, *70*, 6922−6942.
(102) Marquis, R. E.; Clock, S. A.; Mota-Meira, M. Fluoride and Organic Weak Acids as Modulators of Microbial Physiology. *FEMS Microbiol. Rev.* **2003**, *26*, 493−510.
(103) (a) Cherrington, C. A.; Hinton, M.; Mead, G. C.; Chopra, I. Organic Acids: Chemistry, Antibacterial Activity and Practical Applications. *Adv. Microb. Physiol.* **1991**, *32*, 87−108. (b) Brul, S.; Coote, P. Preservative Agents in Foods: Mode of Action and Microbial Resistance Mechanisms. *Int. J. Food Microbiol.* **1999**, *50*, 1−17.
(104) Veeralakshmi, S.; Nehru, S.; Arunachalam, S.; Kumar, P.; Govindaraju, M. Study of Single and Double Chain Surfactant-Cobalt(III) Complexes and Their Hydrophobicity, Micelle Formation, Interaction with Serum Albumins and Antibacterial Activities. *Inorg. Chem. Front.* **2014**, *1*, 393−404.
(105) Damena, T.; Zeleke, D.; Desalegn, T.; Demissie, T. B.; Eswaramoorthy, R. Synthesis, Characterization, and Biological Activities of Novel Vanadium(IV) and Cobalt(II) Complexes. *ACS Omega* **2022**, *7*, 4389−4404.
(106) Carlin, R. L. *Magnetochemistry*; Springer-Verlag: New York, 1986.
(107) Llunell, M.; Casanova, D.; Cirera, J.; Alemany, P.; Alvarez, S. *SHAPE, 2.1*; Universitat de Barcelona: Barecelona, Spain, 2013.
(108) *APEX-II, SAINT-Plus, and TWINABS*; Bruker-Nonius AXS Inc.: Madison, Wisconsin, USA, 2004.
(109) Sheldrick, G. M. *SADABS. Program for Multi-Scan Absorption Correction of Area Detector Data*; University of Göttingen: Germany, 2002.
(110) Altomare, A.; Burla, M. C.; Camalli, M.; Cascarano, G. L.; Giacovazzo, C.; Guagliardi, A.; Moliterni, A. G. G.; Polidori, G.; Spagna, R. *SIR*97: A New Tool for Crystal Structure Determination and Refinement. *J. Appl. Crystallogr.* **1999**, *32*, 115−119.
(111) Sheldrick, G. M. Crystal Structure Refinement with SHELXL. *Acta Crystallogr. C Struct. Chem.* **2015**, *71*, 3−8.
(112) *International Tables for Crystallography, Vol C, Tables 6.1.1.4, 4.2.6.8, and 4.2.4.2*; Kluwer: Boston, 1995.
(113) Dolomanov, O. V.; Bourhis, L. J.; Gildea, R. J.; Howard, J. A. K.; Puschmann, H. *OLEX2*: A Complete Structure Solution, Refinement and Analysis Program. *J. Appl. Crystallogr.* **2009**, *42*, 339−341.
(114) Cockerill, F. R. *Methods for Dilution Antimicrobial Susceptibility Tests for Bacteria That Grow Aerobically: Approved Standard*, 10th Edition; Clinical and Laboratory Standards Institute: Wayne, PA 19087, USA, 2015.